EFFECT OF AP-2β DELETION ON AQUEOUS OUTFLOW PATHWAYS

ABSENT SCHLEMM'S CANAL WITH REDUCTION IN INTRAOCULAR

PRESSURE THROUGH UVEOSCLERAL PATHWAY OBSERVED AFTER

CONDITIONAL DELETION OF AP-2β IN THE MOUSE

BY JAPNIT K. DHAM, B.SC. (HONOURS)

A Thesis

Submitted to The School of Graduate Studies

In Partial Fulfillment of the Requirements

For the Degree

Master of Science

MASTER OF SCIENCE (2022)   McMaster University

(Medical Sciences)   Hamilton, Ontario

TITLE: Absent Schlemm's Canal with Reduction in Intraocular
                        Pressure Through Uveoscleral Pathway Observed After
                        Conditional Deletion of AP-2β in the Mouse

AUTHOR: Japnit K. Dham, B.Sc. (Honours) (McMaster
                        University)

SUPERVISOR: Dr. Judith A. West-Mays

NUMBER OF PAGES: x, 72

LAY ABSTRACT

Glaucoma is one of the leading causes of blindness in the world, with an estimated 76 million people affected by it. This number is projected to increase by almost 30% over the next decade. This drastic increase is a threat to healthcare systems and care facilities, as it will put a great strain on the number of resources that can be provided. In addition, age-related visual disability can lead to several other conditions due to increased risk of injury. Irreversible blindness with glaucoma occurs when the retinal ganglion cells in the eye are damaged due to elevated intraocular pressure, which results from a disruption in aqueous humor drainage. Data from this thesis provides important insight into the development of an important aqueous humor drainage structure, Schlemm's canal, and points to the potential of a mutant mouse model as a model for glaucoma.

ABSTRACT

A unique mouse model recently developed in our laboratory (AP-2β TMR-KO) achieves a conditional deletion of transcription factor AP-2β from the developing periocular mesenchyme and its derivatives using MgpCre/loxP technology. These mutants fail to develop SC and exhibit increased IOP, which temporarily reduces with latanaprost treatment. Here we have shown changes in protein and gene expression of various SC markers. Specifically, Prox1 expression was detected in the wildtype at P4, P10, and P14, but was absent in the AP-2β TMR-KO mice at those stages. Klf4 expression was not present in either wildtype or mutant at P4 but was detected at P10 and P14 in the wildtype only. Additionally, decreased gene expression was observed of *Prox1*, *Klf4*, and *Tie2* in the SC region at P4 and P10, and of *Angpt1* in the trabecular meshwork region, in mutant eyes. Furthermore, dextran tracer studies were performed to assess aqueous outflow in wildtype and AP-2β TMR-KO mice; dextran was detected in regions of both outflow pathways in the wildtype but was clustered in the anterior chamber in the mutant, with the corrected total fluorescence significantly higher in the anterior chamber and significantly lower in regions of outflow for the mutant relative to wildtype. Upon latanaprost treatment, dextran was similarly present in the wildtype, but detected further along the uveoscleral pathway in the mutant with time. The data generated in this project provides more insight into the role of AP-2β in the development and function of the aqueous humor outflow pathways. This information will be critical to elucidating the genetic cascade through which AP-2β regulates anterior segment development. Additionally, this project points to the potential of the AP-2β TMR-KO mice as a model for glaucoma.

ACKNOWLEDGEMENTS

to thank my best friends, Ganeem Juneja and Irzam Gondal. You guys have helped me become a better version of myself, and I am so glad I can rely on you two for anything. I don't know where I would be without my friends and my family, and I am extremely grateful to have such a fantastic support system.

My six years at McMaster have been a roller coaster ride of emotions, and as my time here draws to an end, I want to deeply thank the school and the people here for making these years the best of my life.

TABLE OF CONTENTS

LIST OF TABLES AND FIGURES

LIST OF ABBREVIATIONS

AP-2	Activating Protein 2	Lmx1b	LIM Homeobox Transcription Factor 1-beta
Angpt1	Angiopoietin-1	LVP	Limbal Vascular Plexus
ASD	Anterior Segment Dysgenesis	LEC	Lymphatic Endothelial Cell
AP-2β TMR-KO	AP-2β Trabecular Meshwork Region Knockout	Mgp	Matrix Gla Protein
ARVO	Association for Research in Vision and Ophthalmology	NCC	Neural Crest Cell
BEC	Blood Endothelial Cell	Pitx2	Paired-Like Homeodomain 2
E	Embryonic Day	PFA	Paraformaldehyde
Foxc1	Forkhead Box C1	POM	Periocular Mesenchyme
GWAS	Genome Wide Association Study	PKG	Phosphoglycerokinase
H&E	Hematoxylin & Eosin	PCR	Polymerase Chain Reaction
IGF-BP5	Insulin-Like Growth Factor Binding Protein 5	P	Postnatal Day
IZ	Intermediate Zone	Prox1	Prospero Homeobox Protein 1
IOP	Intraocular Pressure	RV	Radial Vessel
JCT	Juxtacanalicular Tissue	rSC	Rudimentary Schlemm's Canal
Klf4	Kruppel Like Factor 4	SC	Schlemm's Canal

SNP	Single Nucleotide Polymorphism	VEGF	Vascular Endothelial Growth Factor
Tie2	Tunica Interna Endothelial Cell Kinase 2	VEGFR	Vascular Endothelial Growth Factor Receptor
VECAD	Vascular Endothelial Cadherin		

CHAPTER 1

GENERAL INTRODUCTION

1.1. The Anterior Segment of the Eye

Optimal functioning of the visual system is dependent on the retina, which converts light into electrical signals that are subsequently transferred to the brain. In order for the retina to operate correctly, it is necessary for several highly differentiated structures in the anterior segment of the eye to function effectively and in conjunction. These include the cornea, the iris, the lens, the ciliary body, the trabecular meshwork, and Schlemm's canal (SC) (Figure 1). The cornea and the lens both function to provide transparency and
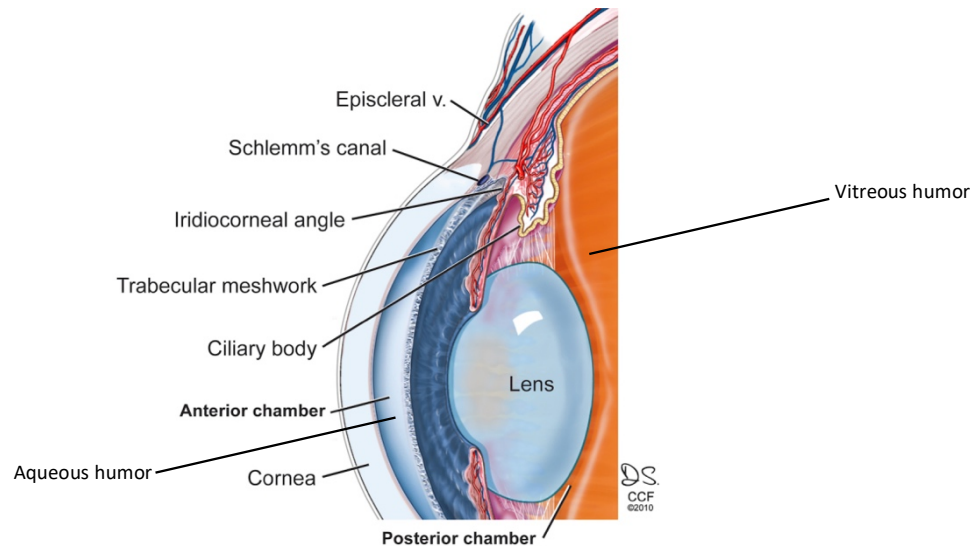
Figure 1. Anatomy of the anterior segment of the eye. A schematic depicting ocular anterior segment anatomy. The structures in the anterior segment include the cornea, iris, lens, ciliary body, trabecular meshwork, and Schlemm's canal. Adapted from (Bollinger et al., 2012).

refraction; the cornea controls and focuses the entry of light into the eye whereas the lens further focuses the light onto the retina. The iris regulates how much light is focused onto the retina, and the ciliary body secretes aqueous humor, a clear fluid which provides nutrition for the cornea and lens, as both are avascular structures (Cvekl & Tamm, 2004). Aqueous humor is secreted by the ciliary body into the posterior chamber of the anterior segment, from where it flows through the pupil into the anterior chamber. It then exits the

eye through two outflow pathways: the conventional pathway and the unconventional/uveoscleral pathway (Figure 2). In the conventional pathway, the aqueous flows through the trabecular meshwork, the juxtacanalicular tissue (JCT), and lastly through SC from where it exits into connecting episcleral veins. The remaining aqueous humor flows out through the uveoscleral pathway, where it passes through the ciliary muscle to exit out from the supraciliary and suprachoroidal spaces (Braunger et al., 2015). The trabecular meshwork and SC provide resistance against aqueous humor, which creates the intraocular pressure (IOP). Optimal IOP is necessary to stabilize the shape of the eye and maintain appropriate distance between the different ocular structures (Cvekl & Tamm, 2004).
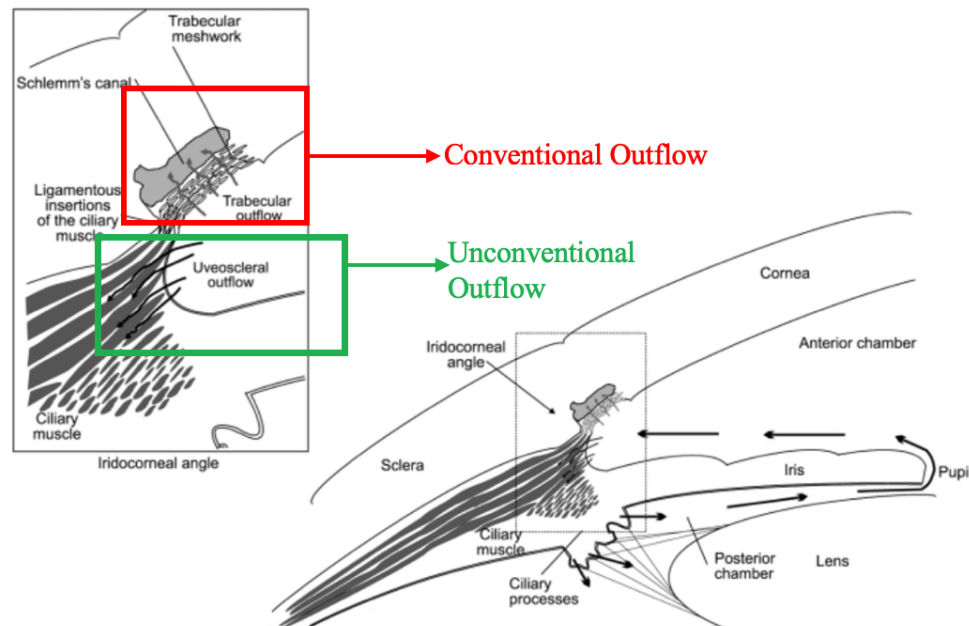
Figure 2. Conventional and unconventional pathways of aqueous humor outflow. Aqueous humor is formed in the ciliary processes from arterial blood, and is secreted to the posterior chamber, where it crosses the pupil to reach the anterior chamber. The inset of the iridocorneal angle shows a close-up of the two pathways of aqueous humor outflow. In the trabecular or conventional pathway, aqueous humor flows through the trabecular meshwork and into Schlemm's canal. In the uveoscleral or unconventional pathway, aqueous humor flows out from the supraciliary spaces and suprachoroidal spaces. Adapted from (Llobet et al., 2003).

1.2. Development of the Anterior Segment

The development of the eye in mammals begins with the bilateral evagination of the diencephalon, resulting in the appearance of the optic pit, the first morphological indication of eye development (Chow & Lang, 2001). The optic pit evaginates further to form the optic vesicles, which extend towards the surface ectoderm (Figure 3A) (Gould et
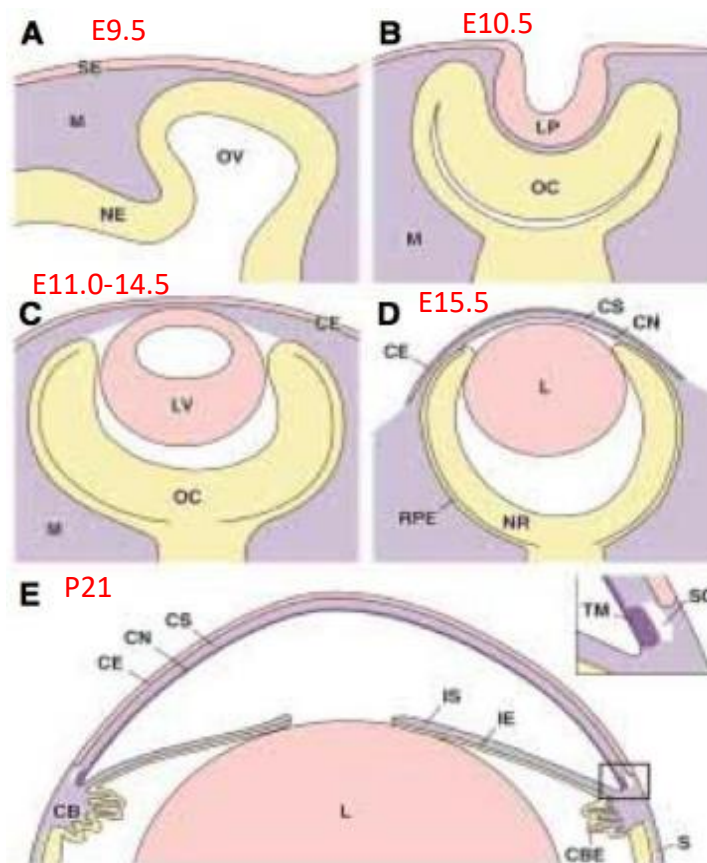
Figure 3. Early development of the mouse eye. (*A*) Formation of the optic vesicle (OV) occurs as it evaginates from the diencephalon, moves through the mesenchymal (M) cells, and reaches the surface ectoderm (SE). (*B*) The SE thickens to form the lens placode and invaginates with the OV to form the optic cup (OC) and lens pit (LP). (*C*) The lens vesicle (LV) is formed when the LP detaches from the SE, which forms the future corneal epithelium (CE). (*D*) The migrating periocular mesenchyme gives rise to the corneal stroma (CS) and corneal endothelium, and the OC forms the neural retina (NR) and retinal pigmented epithelium (RPE). (*E*) The anterior rim of the OC gives rise to the iris epithelium (IE) and ciliary body epithelium (CBE). The periocular mesenchyme gives rise to the ciliary body (CB), trabecular meshwork (TM) and Schlemm's canal (SC). Adapted from (Gould et al., 2004).

al., 2004). The close interaction of the optic vesicles and the surface ectoderm results in the displacement of the periocular mesenchyme (POM). This critical period in development, during which important inductive signals are exchanged between the optic vesicles and the surface ectoderm, occurs at embryonic day 9.5 (E9.5) in the mouse (Chow & Lang, 2001; Gould et al., 2004). The POM is a population of cells derived primarily from the neural crest cells (NCC) with a smaller contribution from the paraxial mesoderm cells (Gage et al., 2005). The interaction between the optic vesicles and surface ectoderm also causes a local thickening in the surface ectoderm, known as the lens placode, while inducing the neural ectoderm to prompt the formation of the retinal placode (Figure 3B). The lens placode proliferates by E10.5 to first form the lens pit and then the lens vesicle (Figure 3C). The lens pit is invaginated at the same time that the neural ectoderm folds to form the optic cup, whereas the lens vesicle remains attached to the surface ectoderm by the lens stalk until it detaches at E11.0. The optic cup becomes the future neural retina and contributes to parts of the anterior segment such as the iris epithelium and ciliary body (Gould et al., 2004).

Soon after the lens vesicle detaches from the surface ectoderm, by E11.0, the first wave of POM cells begins migrating between the anterior lens epithelium and the surface ectoderm leading to the presence of 4-7 layers of mesenchymal cells by E12.0 (Figure 4A-B) (Cvekl & Tamm, 2004). By E12.5, the corneal epithelium has developed and consists of 1-2 layers of the surface ectoderm. The second wave of POM cells migrates over the next two days between the corneal epithelium and the anterior lens epithelium to lay foundation for the future corneal stroma and corneal endothelium (Figure 3D) (Gould et

al., 2004). It has been proposed that the development of the corneal endothelium by E14.5-15.5 is a requirement for the formation of the anterior chamber (Reneker et al., 2000). At this point, the anterior rim of the pigmented optic cup begins to extend anteriorly and
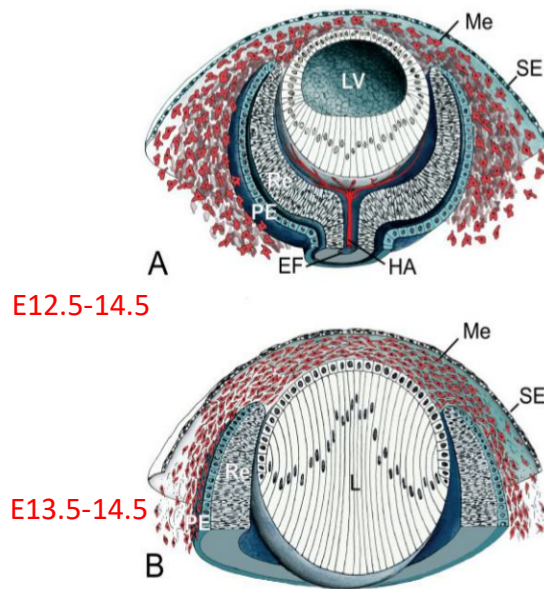
Figure 4. Migration of the POM cells in the developing mouse eye. (*A*) After the detachment of the lens vesicle (LV) from the surface ectoderm (SE), the space between them fills with migrating mesenchymal (Me) cells (Re; neural retina, PE; retinal pigmented epithelium, HA; hyaloid artery, EF; embryonic (choroidal) fissure). (*B*) Me cells form many condensed and flat layers, separated by loose fibrillar extracellular matrix. Adapted from (Cvekl & Tamm, 2004).

centrally, providing a base for the POM which will form the iris stroma and ciliary body stroma. By E16.5, the shape of the anterior chamber is formed (Gould et al., 2004).

The final structures to undergo differentiation in the anterior segment are the aqueous humor outflow structures, the trabecular meshwork and SC, both of which develop in the angle between the iris and the cornea known as the iridocorneal angle. By E17-19, mesenchymal cells fill the iridocorneal angle, interacting with extracellular fibers to leave small spaces (Figure 5). The extracellular fibers then become organized into lamellae covered by flat endothelial-like cells, thus forming the trabecular meshwork. The mature
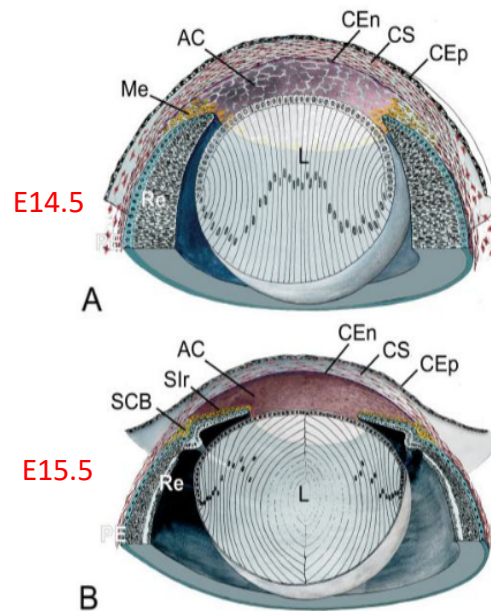
Figure 5. Development of the anterior segment in the mouse eye. (***A***) The corneal stroma (CS) and corneal endothelium (CEn) are derived from the mesenchymal (Me) cells that migrate between the corneal epithelium (CEp) and the lens (L). (***B***) The anterior rim of the optic cup gives rise to the epithelia of the iris and ciliary body, while the Me cells will form the iris stroma (SIr) and ciliary body stroma (SCB) (AC; anterior chamber). Adapted from (Cvekl & Tamm, 2004).

trabecular meshwork is fully formed by postnatal day 21 (P21) (Figure 3E) (Cvekl & Tamm, 2004).

1.3. Anatomy and Development of Schlemm's Canal

First identified in 1830 by Friedrich Schlemm, SC is a unique vessel-like structure lined with endothelial cells that is critical for the outflow of aqueous humor from the eye (Ramos et al., 2007). It is divided into the inner and outer wall, with the former being situated directly adjacent to the JCT of the trabecular meshwork (Figure 6) (Lutjen-Drecoll
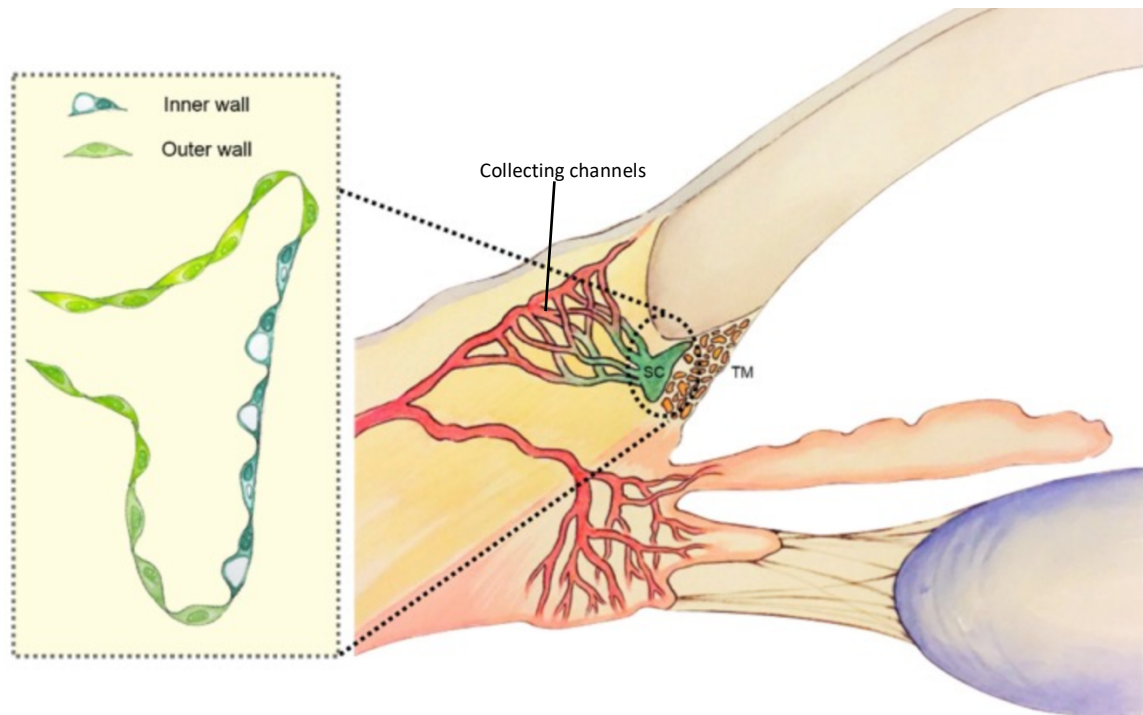
Figure 6. Schematic of the iridocorneal angle region. The inner wall of SC lies adjacent to the trabecular meshwork. Inset shows a magnified view of the morphological differences between the inner and outer SC walls. Adapted from (Dautriche et al., 2015).

& Rohen, 1970). The inner and outer walls of SC differ in terms of morphology and genes expressed. However, the inner wall has been studied much more extensively as it creates the greater resistance to aqueous humor flow since it lines the trabecular meshwork

(Dautriche et al., 2015). The endothelium of the inner wall rests on a discontinuous basement membrane and similarly to lymphatic endothelium, regulates flow in a basal-to-apical direction (Grierson et al., 1978). Due to their location against the JCT, the cells of the inner wall reside in a unique biomechanical environment that shapes their microarchitecture as such. Consequently, these endothelial cells consist of pores and giant vacuoles in addition to F-actin arrangements different from those of the outer wall (Ethier et al., 2004). Outer wall endothelium differs from that of the inner wall due to the presence of Weibel-Palade bodies (small storage granules), a positive desmin stain, as well as a strong affinity for Factor VIII-related antigen (Hamanaka et al., 1992; Hamanaka et al., 1997; Kaufman et al., 2022). Unlike inner wall endothelium, outer wall endothelial cells exhibit stellate actin arrangements (Ethier et al., 2004).

The development of SC occurs in four stages: SC progenitor cell-fate specification, lateral sprouting, lumenization, and separation from venous vasculature (Dautriche et al., 2015). While the POM cells that give rise to other structures in the anterior segment originate from the NCCs, the population that leads to the development of SC is derived from the paraxial mesoderm cells (Gage et al., 2005; Kizhatil et al., 2014). Vessels begin forming in the scleral region adjacent to the iridocorneal angle by E17-19, which will eventually unite to form the elongated SC in continued postnatal development (Cvekl & Tamm, 2004). This network of vessels was defined by Kizhatil and colleagues as the limbal vascular plexus (LVP), which by P1 runs completely around the eye near the external ocular surface (Kizhatil et al., 2014). Another vascular bed deeper within the limbus was defined as radial vessels (RVs), and the region between these two vascular beds is where

SC will form; this region was termed the intermediate zone (IZ). Endothelial sprouts originating from both the LVP and RV begin entering the IZ by P1, the leading cells of which exhibit characteristic tip cell morphology with long filopodia; tip cells are a subtype of endothelial cells crucial for angiogenesis (Kizhatil et al., 2014). Similarly, to angiogenesis, SC tip cells interact using their filopodia which is monitored by macrophages, while vascular endothelial cadherin (VECAD) makes adhesive contacts between the tip cells. The adhered tip cells connect in the IZ and produce tip cell clusters. Between P3-P4, the clusters conjoin to form a flattened line of cells, termed the rudimentary SC (rSC), which remains connected to the LVP and RV (Kizhatil et al., 2014).

The presence of prospero homeobox protein 1 (Prox1) in SC was first demonstrated by Truong and colleagues; Prox1 expression in blood endothelial cells (BECs) is critical for the induction of lymphatic endothelial cells (LECs), deeming it the master regulator of lymphatic fate (Park et al., 2014; Truong et al., 2014). It has been suggested that Prox1 works cooperatively with Kruppel like factor 4 (Klf4), a transcription factor which is a key responder to shear stress (McCormick et al., 2001). Prox1 expression in the rSC begins between P4-P5, where regions with increasingly positive expression exhibit increasing tubular morphology suggesting that Prox1 expression correlates with the transition from flat cells to a tube-like structure. By P9, most SC cells express Prox1 and by P10, formation of the lumen as well as differentiation to a mature architecture begins to occur at some locations. Prox1 expression in cells of the outer wall of SC begins decreasing at this point (Kizhatil et al., 2014). SC continues to develop and grow until approximately P21 (Cvekl & Tamm, 2004).

The exact mechanism and signaling cascade that leads to the development of SC is not yet fully understood. However, some key markers and regulatory molecules have been recently identified. It has been demonstrated that vascular endothelial growth factor (VEGF)-C is required for the migration of BECs and lateral sprouting from scleral veins (Aspelund et al., 2014). BECs that serve as progenitors for SC express VEGF receptor (VEGFR)-2 as well as tunica interna endothelial cell kinase (Tie) 2 receptor (Aspelund et al., 2014; Park et al., 2014). The growth factor angiopoietin 1 (Angpt1) is an important ligand of the Tie2 receptor; it is expressed in the trabecular meshwork and its release has been demonstrated to be crucial for SC development (Thomson et al., 2021).

1.4. Anterior Segment Dysgenesis and Glaucoma

Anterior segment dysgenesis (ASD) is a group of disorders involving several different structures including the iris, cornea, lens, trabecular meshwork, and SC. In most of these disorders, one or more of these structures develop abnormally due to genetic mutations. Some of these disorders include Axenfeld's anomaly, Rieger's anomaly, Peter's anomaly, aniridia, iris hypoplasia, and iridogoniodysgenesis. Mutations in several genes have been discovered till date which are known to contribute to different types of ASD disorders. These include *PAX6, PITX2, PITX3, FOXC1, FOXE3, EYA1, CYP1B1, LMX1B*, and *MAF*. Since patients with ASD often develop malformations in tissues that regulate IOP and control aqueous humor drainage, they are at high risk for developing glaucoma (Gould & John, 2002).

Glaucoma is the second leading cause of blindness in the world, with an estimated 76 million people affected worldwide (Quigley & Broman, 2006). It is a complex disease

characterized by the loss of retinal ganglion cells, visual field defects, and degeneration of the optic nerve. There are two main types of glaucoma associated with ASD: open angle glaucoma and closed angle glaucoma (Gould & John, 2002). The main difference between the two types is that in closed angle glaucoma, the iridocorneal angle is at least 75% closed due to the adherence of the iris and the cornea (Weinreb et al., 2014).

Treatment for glaucoma primarily targets the elevated IOP commonly observed in the disease; it is currently the only modifiable factor of the disease that successfully reduces risk of disease onset and progression (Chang & Goldberg, 2012). Although the uveoscleral pathway does not contribute to the IOP, it can be utilized to lower it in disease through the use of prostaglandin analog drugs, such as latanoprost, which have been demonstrated to increase aqueous outflow through the uveoscleral pathway (Alm & Stjernschantz, 1995).

1.5. Critical Genes for Anterior Segment Development in the POM

The development of many anterior segment structures is governed by the POM. As a result, many of the genes implicated in different ASD disorders and glaucoma are expressed in the POM including transcription factors forkhead box C1 (Foxc1), paired-like homeodomain 2 (Pitx2), and LIM homeobox transcription factor 1 beta (Lmx1b). These genes have previously been studied using various animal models and genetic modification techniques.

The gene *Foxc1*, which encodes the transcription factor Foxc1, is normally expressed in the POM at E11.5 and is subsequently downregulated in parallel with differentiation of the corneal endothelium. In a mouse model homozygous null for *Foxc1*, the mutant animals exhibit a mutant lens adhered to the cornea, resulting in the absence of

the anterior chamber. The corneal endothelium was missing as well, while the corneal stroma was disorganized and the corneal epithelium thicker than usual (Kidson et al., 1999). These defects were observed embryonically as these mice did not survive after birth. However, mice heterozygous for *Foxc1* survived postnatally and exhibited less severe defects. Specifically, the study revealed closed angle phenotypes with an underdeveloped or absent Schlemm's canal and an abnormally developed trabecular meshwork, cloudy corneas, and iris hypoplasia (Smith et al., 2000).

Another gene of interest, *Pitx2*, is expressed in the POM beginning E9.5 and expression continues in ocular structures including the presumptive cornea, iris, and iridocorneal angle (Gage et al., 1999). In a mouse model homozygous null for *Pitx2*, defects such as an absent corneal endothelium and anterior chamber, as well as a thick and undifferentiated corneal epithelium, were observed; these mice did not survive past E15.5 (Gage et al., 1999; Lin et al., 1999). Both *Pitx2* and *Foxc1* have been implicated in Axenfeld-Rieger syndrome, an autosomal dominant ASD disorder that also presents with other systemic abnormalities (Berry et al., 2006). Studies have shown these genes to be dosage responsive, and functional interactions between the two seem to underlie the sensitivity to *Foxc1* gene dose in Axenfeld-Rieger syndrome (Berry et al., 2006; Gage et al., 1999).

Nail patella syndrome (NPS), another type of ASD disorder, can be caused by mutations in the *Lmx1b* gene (McIntosh et al., 1998). *Lmx1b* is first detectable in the POM beginning at E10.5 and in a mouse model homozygous null for *Lmx1b*, defects such as reduced ocular size, iris and ciliary body hypoplasia, and decrease in density of corneal

keratocytes were shown. Interestingly, the normal ocular expression pattern of *Pitx2* is almost identical to that of *Lmx1b*, while *Foxc1* is expressed in an overlapping pattern with the two in the POM. In the *Lmx1b* homozygous null mutants, *Pitx2* expression remains unaffected. However, *Foxc1* levels are increased, suggesting *Lmx1b* may directly or indirectly regulate *Foxc1* expression (Pressman et al., 2000). In mutants homozygous null for *Pitx2*, subtle differences in *Lmx1b* expression have been reported. However, it remains unclear whether that is directly due to changes in *Pitx2* expression (Lin et al., 1999).

Recent analysis from a genome-wide association study (GWAS) has demonstrated that single nucleotide polymorphisms (SNPs) for the gene *Tfap2b* may be associated with glaucoma in humans (Dr. J. Wiggs, personal communication). *Tfap2b* encodes the transcription factor activating protein-2 (AP-2)β (Eckert et al., 2005).

1.6. Family of Activating Protein-2 Transcription Factors

The family of transcription factors known as the activating protein-2 (AP-2) family consists of five members in humans and mice: AP-2α, AP-2β, AP-2γ, AP-2δ and AP-2ε, which are encoded by the genes *Tfap2a, Tfap2b, Tfap2c, Tfap2d,* and *Tfap2e,* respectively (Eckert et al., 2005). All of these retinoic acid-responsive transcription factors are encoded by 7 exons in mammals and share a characteristic domain structure, with the exception of AP-2δ (Eckert et al., 2005; West-Mays et al., 1999). They share a highly conserved helix-span-helix dimerization motif at the carboxyl terminal, followed by a basic central region, which is then followed by a less conserved proline and glutamine rich domain at the amino terminal (Figure 7). The helix-span-helix motif in conjunction with the basic region binds DNA, while the proline and glutamine rich amino terminal mediates transactivation (Eckert

et al., 2005). It has been demonstrated that homodimerization and integrity of the central

basic region are required for DNA binding; the basic and first helical domains are encoded

by parts of exons 4, 5, and 6 (Bauer et al., 1994; Hilger-Eversheim et al., 2000; Wankhade

et al., 2000).

It has been demonstrated that the AP-2 proteins bind to the palindromic consensus

sequence 5'-GCCNNNGGC-3' which is found in a variety of cellular and viral enhancers;

additional binding motifs suggest that the AP-2 proteins potentially bind to many different
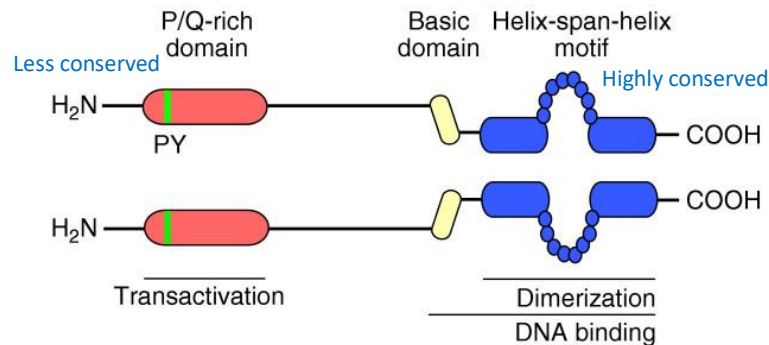
Figure 7. Schematic of AP-2 transcription factors' structure. The AP-2 proteins contain a proline/glutamine rich transactivation domain at the amino terminal, a basic domain, and the helix-span-helix motif at the carboxyl terminal which mediates protein dimerization and DNA binding. Adapted from (Eckert et al., 2005).

G/C rich elements with varying affinities (Eckert et al., 2005; Mohibullah et al., 1999).

Genes which have been found to contain AP-2 binding sites in their promoter sequences,

such as insulin-like growth factor binding protein 5 (IGF-BP5), prothymosin-α, and the

estrogen receptor, are involved in a wide variety of biological functions (Duan &

Clemmons, 1995; Eckert et al., 2005; Gaubatz et al., 1995; Hilger-Eversheim et al., 2000;

Newman et al., 2000). The AP-2 proteins have also been shown to have a regulatory role

in cell cycle control, apoptosis, and differentiation (Hilger-Eversheim et al., 2000).

Three of the five AP-2 transcription factors in mice are expressed in the NCC population, including AP-2α, AP-2β, and AP-2γ (Eckert et al., 2005; Moser, Ruschoff, et al., 1997). Despite this overlap, disruption in these proteins has demonstrated their non-redundant roles in development. Mutations in AP-2α primarily disrupt the cranial neural crest and limb mesenchyme, leading to errors in facial and limb development (Eckert et al., 2005; Schorle et al., 1996; Zhang et al., 1996). AP-2β has been demonstrated to be important for kidney development, while AP-2γ is key for the placentation of the embryo (Eckert et al., 2005; Moser, Pscherer, et al., 1997; Werling & Schorle, 2002). Dominant negative alleles of AP-2β have been elucidated as the cause of Char syndrome, a rare disorder resulting in the persistence of a fetal heart structure even after birth as well as facial dysmorphism and abnormal fifth digits (Eckert et al., 2005; Satoda et al., 2000).

1.7. Activating Protein-2beta

Of the five AP-2 proteins, AP-2α and AP-2β have been shown to play important roles in ocular development (Akula et al., 2020; Bassett et al., 2012; Bassett et al., 2010; Martino et al., 2016; Taiyab et al., 2022; West-Mays et al., 1999). mRNA from *Tfap2b* is found at high levels at E8.5, when the neural crest is emerging from the neural tube, and the gene continues being expressed during the migration of the POM cells that are derived from the NCCs (Mitchell et al., 1991). Consequently, AP-2β is expressed in the structures derived from the POM during its first wave of migration into the anterior segment, the corneal endothelium and the corneal stroma (Martino et al., 2016). Expression of *Tfap2a* is also high at this point in embryogenesis; however, by E15.5, only *Tfap2b* expression is maintained indicating that the expression of AP-2β is also present in the second wave of

migration of the POM cells (Bassett et al., 2010; West-Mays et al., 1999). This points to the importance of AP-2β in the development of ocular structures derived from the POM, such as the corneal endothelium, corneal stroma, ciliary body stroma, iris stroma, and the trabecular meshwork (Akula et al., 2020).

1.8. Conditional Deletion of AP-2β from the Neural Crest

A germline deletion of AP-2β in mice results in perinatal death due to defects in the heart, kidneys, and/or nervous system (Moser, Pscherer, et al., 1997). Therefore, previous research in our laboratory employed a Wnt1Cre transgenic mouse system to achieve a conditional deletion of AP-2β from the NCC population, in which Wnt1Cre expression begins at E8.5 (Lewis et al., 2013; Martino et al., 2016). These mutant mice were termed the AP-2β neural cell knockout (AP-2β NCC-KO) mice, and previous research in our laboratory demonstrated they exhibited several anterior segment defects. Specifically, there was an absence of the corneal endothelium and a complete adherence of the iris to the cornea, resulting in a closed iridocorneal angle, leading to elevated IOP and loss of retinal ganglion cells (Martino et al., 2016). In addition, it was also demonstrated that AP-2β is required for development and differentiation of the trabecular meshwork and SC as both structures were deleted and the expression of critical markers of both structures was absent in the mutant mice. However, it is important to note that although AP-2β is expressed in the trabecular meshwork, it is not normally expressed in SC (Akula et al., 2020).

1.9. Conditional Deletion of AP-2β from the POM

Next, our laboratory employed the use of a MgpCre transgenic mouse system to achieve a more specific deletion of AP-2β from the POM cell population. These mice were termed the AP-2β trabecular meshwork region knockout (AP-2β TMR-KO) mice. The MgpCre mice were obtained from one of our collaborators, Dr. Terete Borras. The expression of MgpCre is confined to the iridocorneal angle and the peripapillary scleral region (Borras et al., 2015). Although the results achieved using the AP-2β NCC-KO mice may indicate a cell-autonomous function of AP-2β in regulating differentiation of the trabecular meshwork, it is possible that the closed-angle phenotype prevented mesenchymal cells from proliferating correctly. Therefore, further experiments were conducted on the AP-2β TMR-KO mice to determine whether the role of AP-2β in trabecular meshwork region differentiation is cell-autonomous or non-cell autonomous. A deletion of the trabecular meshwork region and an underdeveloped SC were observed in addition to a reduction in the expression of key markers (Taiyab et al., 2022). There was only a partial adherence of the iris to the cornea with the iridocorneal angle partially closed, and an elevated IOP was measured (Figure 8). The IOP was found to reduce temporarily through treatment with latanaprost, a prostaglandin analog (Figure 9) (Taiyab et al., 2022). The question remained, however, of how a conditional deletion of AP-2β in both models led to an absent SC since AP-2β is not normally expressed in the structure. Additionally, the reduction in IOP warranted further investigation as the conventional pathway of aqueous humor outflow is blocked in the mutants.
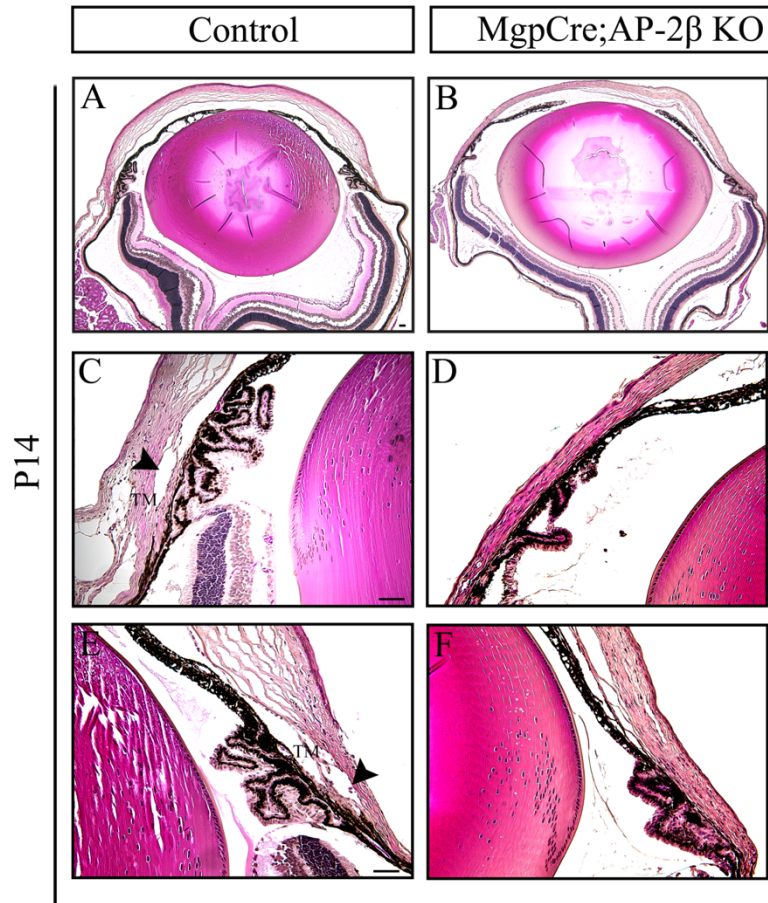
Figure 8. Hematoxylin & Eosin staining of sagittal sections of AP-2β TMR-KO mutants at P14. (*A-B*) There is only a partial adherence of the iris to the cornea in the mutant, but the iridocorneal angle is still closed. (*C-F*) Higher magnification images of A and B demonstrate the absence of the trabecular meshwork (TM) and SC (arrowhead). Scale bars represent 100 μm. Adapted from (Taiyab et al., 2022).
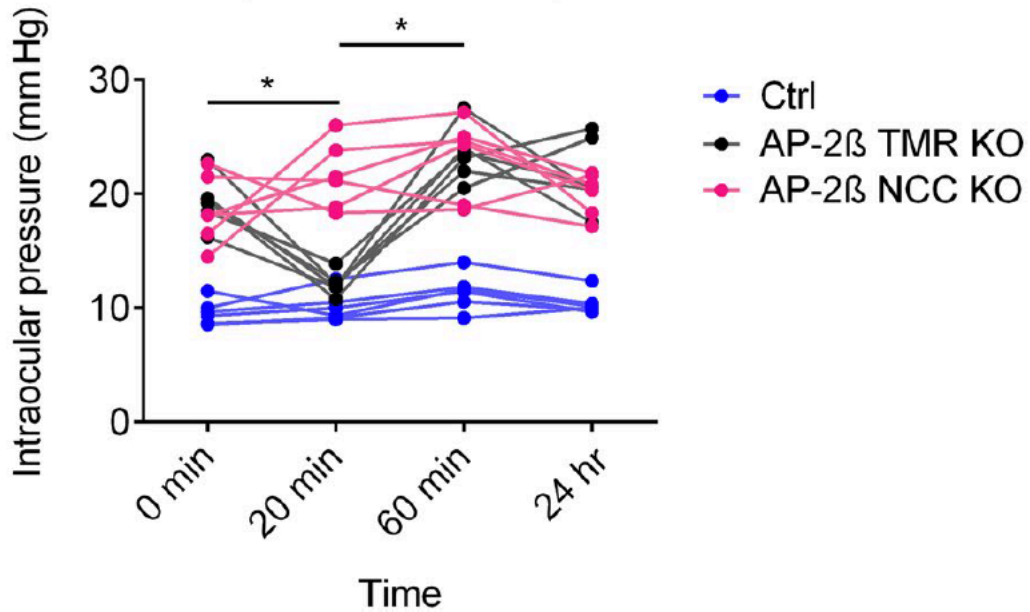
Figure 9. Increased IOP resulting from partial angle closure in AP-2β TMR KO eyes that reduces upon latanoprost treatment. IOP in AP-2β TMR KO mice is significantly lower at 20 minutes after latanoprost treatment (n=6 eyes; p<0.0001; two-way repeated measures ANOVA) when compared to its own baseline IOP. By 60 minutes post-treatment, TMR KO IOP increases significantly compared to the IOP at 20 minutes (p<0.0001). On the other hand, AP-2β NCC KO mice display high IOP both before and after latanoprost treatment (n=6 eyes; p<0.0001 for all time points analyzed compared with controls). Obtained from (Taiyab et al., 2022).

CHAPTER 2

RATIONALE, MAIN HYPOTHESIS, & RESEARCH AIMS

2.1. Rationale for the Study

Adequate development of structures in the anterior segment is critical for proper functioning of the eye. Aberrations in the development of these structures can lead to a wide range of ASD disorders; in approximately 50% of patients, this will lead to the development of glaucoma. In particular, proper development of the aqueous humor outflow structures is necessary to sustain the balance between aqueous humor production and drainage, thus maintaining optimal IOP. An abnormally developed trabecular meshwork or SC can cause buildup of aqueous humor, leading to elevated IOP. Investigating the genetic pathways and mechanisms that govern the proper development of these structures is crucial for a better understanding of the underlying cause of the disease.

An important part of these genetic pathways is the AP-2 family of transcription factors, which has been the focus of our laboratory for a number of years. We have generated different animal models to study the role these transcription factors play in anterior segment development. A germline deletion of AP-2β results in mouse death perinatally. Consequently, our researchers have recently demonstrated that a conditional deletion of AP-2β from the developing POM using MgpCre/loxP technology leads to defects in many different ocular structures, including an absent trabecular meshwork and SC. An elevated baseline IOP was also measured, which was found to reduce temporarily through treatment with a prostaglandin analog drug, latanaprost.

Investigating the effect that a conditional deletion of AP-2β has on the development of SC, even though it is not expressed in it, will allow for a better understanding of an ocular structure about which there is very little currently known. Additionally,

investigating the temporary reduction in IOP upon latanaprost treatment will provide further insight on the relationship between AP-2β and the outflow pathways of aqueous humor, with the potential to make the AP-2β TMR-KO mice a suitable animal model for glaucoma.

2.2. Main Hypothesis

AP-2β deletion from the POM disrupts SC morphology and function by influencing the expression of key SC developmental markers.

2.3. Research Aims

2.3.1. Evaluate expression of various markers of SC at important time-points in development in the AP-2β TMR-KO mice and compare to control littermates.

In previous research conducted in our laboratory, histological staining of AP-2β TMR-KO eyes lacks a vessel-like structure indicative of SC at P14. The present research seeks to further investigate the defects observed in SC by studying the expression of key markers. Histological examination of wild-type and AP-2β TMR-KO eyes will be done at important time-points in development, including P4, P7, P10, and P14. Immunohistochemical staining will be performed to stain for Prox1 and Klf4 in wild-type and AP-2β TMR-KO eyes at the same time-points; both proteins have previously been proven to be expressed in SC. Additionally, gene expression of important SC regulators including *Prox1*, *Klf4*, *Tie2*, and *Angpt1* will be investigated in conjunction with other genes using a new RNAscope HiPlex technique.

2.3.2. Assess the functionality of the uveoscleral outflow pathway in the AP-2β TMR-KO mice and determine if it is being used to reduce IOP.

Previous studies in our laboratory have revealed a significant increase in the baseline IOP of AP-2β TMR-KO mice relative to control littermates at P30, which was temporarily reduced with latanaprost treatment. Since the conventional pathway is blocked in these mutants, we suspect that this reduction in IOP is due to increased outflow through the uveoscleral pathway, which we hypothesize remains unaffected by AP-2β deletion. In order to test this, intracameral injections with a dextran tracer will be performed on AP-2β TMR-KO and wild-type eyes, both untreated and treated with latanaprost. The outflow of aqueous humor will be visualized using fluorescence microscopy, and the corrected total fluorescence in the anterior chamber and trabecular meshwork region will be compared between AP-2β TMR-KO and wild-type mice.

CHAPTER 3

EXPERIMENTAL DESIGN

3.1. Animal Husbandry

All animal procedures were performed in accordance with the Association for Research in Vision and Ophthalmology (ARVO) statement for the use of animals in ophthalmic and vision research. All experiments were performed at McMaster University, with animals housed in the Central Animal Facility. Ear or tail clippings were taken for genotyping, and DNA extraction was performed using the EZNA Tissue DNA Kit (Omega Bio-Tek). Genotyping was performed using standard polymerase chain reaction (PCR) protocols (Table 1).

Table 1. PCR Protocols for genotyping of AP-2β TMR-KO mice

Alleles	Primers	PCR Conditions	Products
MgpCre	**Cre1** 5'-GCT GGT TAG CAG CGC AGG TGT AGA G-3' **Cre3** 5'-CGC CAT CTT CCA GCA GGC GCA CC-3'	33 cycles of: 45 seconds at 95 °C 1 minute at 67 °C 1 minute 10 sec at 72 °C	Cre transgene present at 420 bp
Tfap2b	**4 Exon DW** 5'-CCT CCC AAA TCT GTG ACT TCT-3' **PGK-PolyA** 5'-CTG CTC TTT ACT GAA GGC TCT TT-3' **4 Exon Rev** 5'-TTC TGA GGA CGC CCA GG-3'	37 cycles of: 45 sec at 95 °C 45 sec at 58 °C 1 min at 72 °C	Tfap2b$^-$ at 380 bp Tfap2b$^+$ at 221 bp

3.2. Generation of AP-2β TMR-KO Mice

To generate the AP-2β TMR-KO mice, two mouse lines were first created to begin the breeding process. In one line, the *Tfap2b* gene contained a null allele (*Tfap2b$^{+/-}$*) using a germline insertion of phosphoglycerokinase (PKG) neo cassette to disrupt exon 4 (Moser, Pscherer, et al., 1997). In the second line, exon 4 of *Tfap2b* was flanked by loxP sites (*Tfap2b$^{lox/lox}$*). Additionally, a third line was obtained from our collaborator, Dr. Terete Borrás, where the enzyme Cre recombinase is expressed under control of the promoter for the Matrix Gla Protein (*Mgp*) gene (*Mgp*-Cre.KI$^{+/-}$) (Borras et al., 2015). In the first cross, female *Tfap2b$^{+/-}$* mice were bred with male *Mgp*-Cre.KI$^{+/-}$ mice to generate *Tfap2b$^{+/-}$*;*Mgp*-Cre.KI$^{+/-}$ mice. Male offspring with that genotype were bred with female *Tfap2b$^{lox/lox}$* mice to produce the final mutants, *Tfap2b$^{-/lox}$*;Mgp-Cre.KI$^{+/-}$, in addition to control littermates; these mutants have been named the AP-2β TMR-KO mice. Their genome contains one active copy of *Tfap2b* in all cells, except for *Mgp*-expressing cells, in which exon 4 of the second copy is excised by Cre recombinase to render a conditional deletion of AP-2β. It is important to note that the Cre transgene was passed on by male breeders in all crosses to minimize differences in Cre recombinase activity due to parent-of-origin, as has been reported previously (Heffner et al., 2012). The breeding scheme used to generate the AP-2β TMR-KO mutants is depicted in Figure 10. For the final genetic crosses, inbreeding was avoided, and the background strain used for all genetic crosses was C57BL/6J (Charles River, Wilmington, MA).
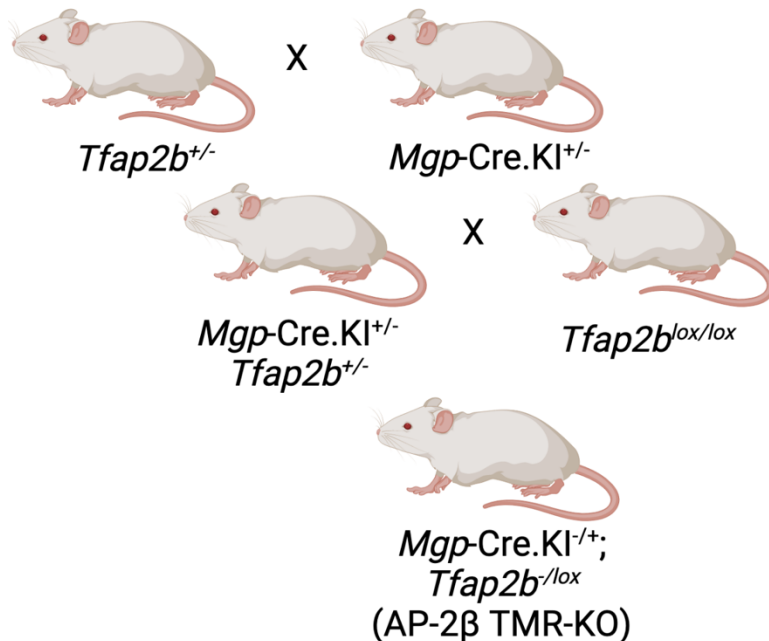
Figure 10. Generation of AP-2β TMR-KO mutants. *Mgp*-Cre.KI$^{+/-}$ mice are bred with *Tfap2b*$^{+/-}$ mice. Male *Mgp*-Cre.KI$^{+/-}$;*Tfap2b*$^{+/-}$ offspring are then bred with female *Tfap2b*$^{lox/lox}$ mice to obtain the final offspring, the *Mgp*-Cre.KI$^{+/-}$;*Tfap2b*$^{-/lox}$ mice or AP-2β TMR-KO, in addition to littermate controls.

3.3. Histology

Eyes were enucleated from euthanized AP-2β TMR-KO mice, as well as control littermates. The dissected eyes were fixed in 4% paraformaldehyde (4% PFA) for 24 hours at 4 ºC for staining and immunohistochemistry or 2% PFA for 3 hours at room temperature for dextran tracing and then preserved in 70% ethanol at 4 ºC for paraffin sections, or 30% sucrose overnight at 4 ºC for cryosections. The eyes were then sent to McMaster University's facility for processing and embedded in paraffin wax (Paraplast tissue embedding media, Fisher Scientific, Waltham, MA) or optimal cutting temperature medium. The paraffin blocks were subsequently sectioned into 4 μm thick sections for hematoxylin & eosin (H&E) or immunohistochemical staining and 6 μm thick for dextran

tracing, while frozen tissue was cryosectioned into 10 μm thick sections for RNAscope studies (Bassett et al., 2007; Lindsey & Weinreb, 2002).

3.4. Immunohistochemistry

The paraffin sections were deparaffinized in a series of xylene washes and rehydrated through washes with decreasing concentrations of ethanol, ending in a final water wash. For antigen retrieval, the sections were immersed in 80-90 °C 10 mM sodium citrate for 20 minutes, followed by a 20-minute period in which they were allowed to return to room temperature. Next, the sections were incubated for 1 hour with blocking serum retrieved from the host animal of the secondary antibody at a concentration of 5% serum diluted in 1xPBS, in order to block non-specific staining. In experiments involving Prox1 staining, the blocking step was performed using a Background Buster solution (Innovex Biosciences) instead of the diluted blocking serum and the sections were incubated for 10 minutes, followed by a rinse in water. The sections were then incubated overnight at 4 °C with the appropriate dilution of primary antibodies in 1xPBS. Primary antibodies include Prox1 (1:100, Covance), endomucin (1:100, eBioscience), and Klf4 (1:200, R&D Systems). The next day, after 2 washes in 1xPBS for 5 minutes each, Alexa Fluor (Invitrogen, Molecular Probes) secondary antibodies were applied at a 1:200 dilution in addition to 1.5% serum, diluted in 1xPBS. The sections were incubated for 1 hour at room temperature, followed by three washes in 0.1% Tween-20 solution in 1xPBS for 5 minutes each. Finally, ProLong Gold mounting medium containing DAPI (Invitrogen, Molecular Probes) was applied. All imaging was performed using a Leica fluorescence light

microscope along with LasX software, and images were reproduced using Adobe Photoshop 2022 (Adobe Systems Inc.).

3.5. HiPlex RNAscope Assay

The assay was performed on frozen ocular tissue within 3 months of enucleation. Slides were washed in 1xPBS for 5 minutes to remove OCT, and then baked at 60 °C for 30 minutes. This was followed by post-fixation in freshly prepared 4% PFA for 30 minutes at room temperature, and dehydration by running the slides through 50%, 70%, and 2x100% ethanol, each for 5 minutes. Target retrieval was performed using a steamer, and slides were immersed in the target retrieval reagent for 3 minutes at 100 °C, after which they were rinsed with 100% ethanol. Once the slides were completely dry, a hydrophobic barrier was drawn, and the sections were treated with protease for 15 minutes at room temperature. Next, the slides hybridized with 12 target probes for minimum 2 hours at 40 °C and washed with 1xwash buffer for 4 minutes, followed by three subsequent amplification steps with the same wash between each. Next, the first set of three fluorophores were hybridized for 15 minutes at 40 °C. DAPI and mounting medium were added to the sections, after which they were cover slipped. Imaging was performed the next day, with images acquired using a Leica microscope with a fluorescence attachment and a high-resolution camera along with LasX imaging software. After imaging, the slides were immersed in 4xSSC until cover slips fell off and incubated twice with 10% cleaving solution for 15 minutes at room temperature, in between which the slides were washed with PBST (0.5% Tween-20) for 4 minutes. The slides were then hybridized with the next set

of fluorophores, and all subsequent steps were repeated until all four sets of fluorophores had been hybridized and imaged (Advanced Cell Diagnostics).

3.6. Dextran Tracing and Image Analysis

Adult AP-2β TMR-KO mice, as well as control littermates, were anesthetized using 2.5% Avertin at 0.15 mL/10 g body weight. Alcaine (Alcon, Mississauga, ON, Canada) was applied as a topical anesthetic, and 1 μL of a 40 kDA lysine-fixable fluorescein-labeled dextran tracer (Sigma Aldrich) was intracamerally injected into the anterior chamber using a Hamilton syringe. When required, animals were treated with latanaprost (0.005%, Xalatan, Pfizer). Animals were euthanized 10 minutes after injection, after which eyes were bathed with 2% PFA, enucleated, and fixed for 3 hours at room temperature in 2% PFA. They were preserved in 70% ethanol for paraffin sections, processed by McMaster University's facility, and embedded in paraffin wax. Paraffin blocks were sectioned at a thickness of 6 μm, cleared in xylenes, rehydrated through a graded ethanol series, and rinsed in 1xPBS. The slides were then exposed to 1% sodium borohydride in 1xPBS for 10 minutes to reduce autofluorescence, rinsed in PBS, and mounted and cover slipped. Imaging was performed with a Leica microscope using a fluorescence attachment, and images were acquired using a high-resolution camera, along with LasX imaging software (Lindsey & Weinreb, 2002). Quantification of the fluorescent signal was performed on the ImageJ (NIH) software, using measurements for Integrated Density, Area, and Mean Gray Value for the anterior chamber and the region of the outflow pathways. Corrected total fluorescence was calculated using the following formula: CTF = Integrated Density – (Area*Mean fluorescence of background).

3.7. IOP Measurements

Adult AP-2β TMR-KO and control littermates were anesthetized with 2.5% Avertin and injected with a 40 kDa dextran tracer as described above. Eye drops (Alcon, Mississauga, ON, Canada) were applied to prevent drying of the cornea. Whiskers were trimmed to prevent interference with the probe and a rebound tonometer (TonoLab, Vantaa, Finland) was used to obtain a minimum of 6 baseline IOP values, with each value automatically generated as an average of 6 measurements (Martino et al., 2016). Topical latanaprost (0.005%, Xalatan, Pfizer) was applied to the eyes and IOP measurements were taken once again 10 minutes after treatment.

3.8. Statistical Analysis

Differences in IOP between control and AP-2β TMR-KO mice of all treatment conditions were analyzed using a 2-way ANOVA with repeated measures on GraphPad Prism 9.0 (La Jolla, CA, USA). Differences in corrected total fluorescence between control and AP-2β TMR-KO mice of all treatment conditions were analyzed using a 2-way ANOVA.

CHAPTER 4

RESULTS

4.1. Aim 1: Evaluate expression of various markers of SC at important time-points in development in the AP-2β TMR-KO mice and compare to control littermates.

4.1.1. Examining protein expression of key SC markers through immunohistochemistry

As demonstrated by previous histological staining, SC appears to be absent in the AP-2β TMR-KO mutants at P14 as compared to wildtype littermates (Figure 8). To investigate this further, I have examined the protein expression of key markers of SC such as Prox1 and Klf4. Immunohistochemical staining of Prox1 co-stained with endomucin, an established marker of endothelial cells, was carried out at various time-points including P4, P7, P10, P14, and P30, in addition to H&E staining in order to examine SC status (data not shown for P7 and P30) (Kizhatil et al., 2014). At P4 (n=4 eyes), no defined structure was observed in either wildtype or mutant, yet nuclear expression of Prox1 was present in the approximate SC region of the wildtype, as displayed through overlay with DAPI and endomucin (Figure 11A-E). This staining pattern was completely absent in the mutant (Figure 11F-H– see asterisks). By P10 (n=4 eyes), a tubular structure was observed in the H&E stain of the wildtype, the endothelium lining SC in the wildtype was detected through endomucin staining, and nuclear Prox1 was observed at much higher levels in the inner SC wall relative to the outer (Figure 12A-D– see rectangles). However, no such structure was present in the mutant, and Prox1 staining was not detected (Figure 12E-H– see asterisks). At P14 (n=4 eyes), the wildtype SC was seen to be more elongated in shape, and nuclear Prox1 was detected primarily in the inner SC wall, with little to none expressed in the outer at this stage (Figure 13A-D– see rectangles). In the mutant, there was no defined vessel-

shaped structure once again, and Prox1 staining was seen to be completely absent (Figure

13E-H– see asterisks).
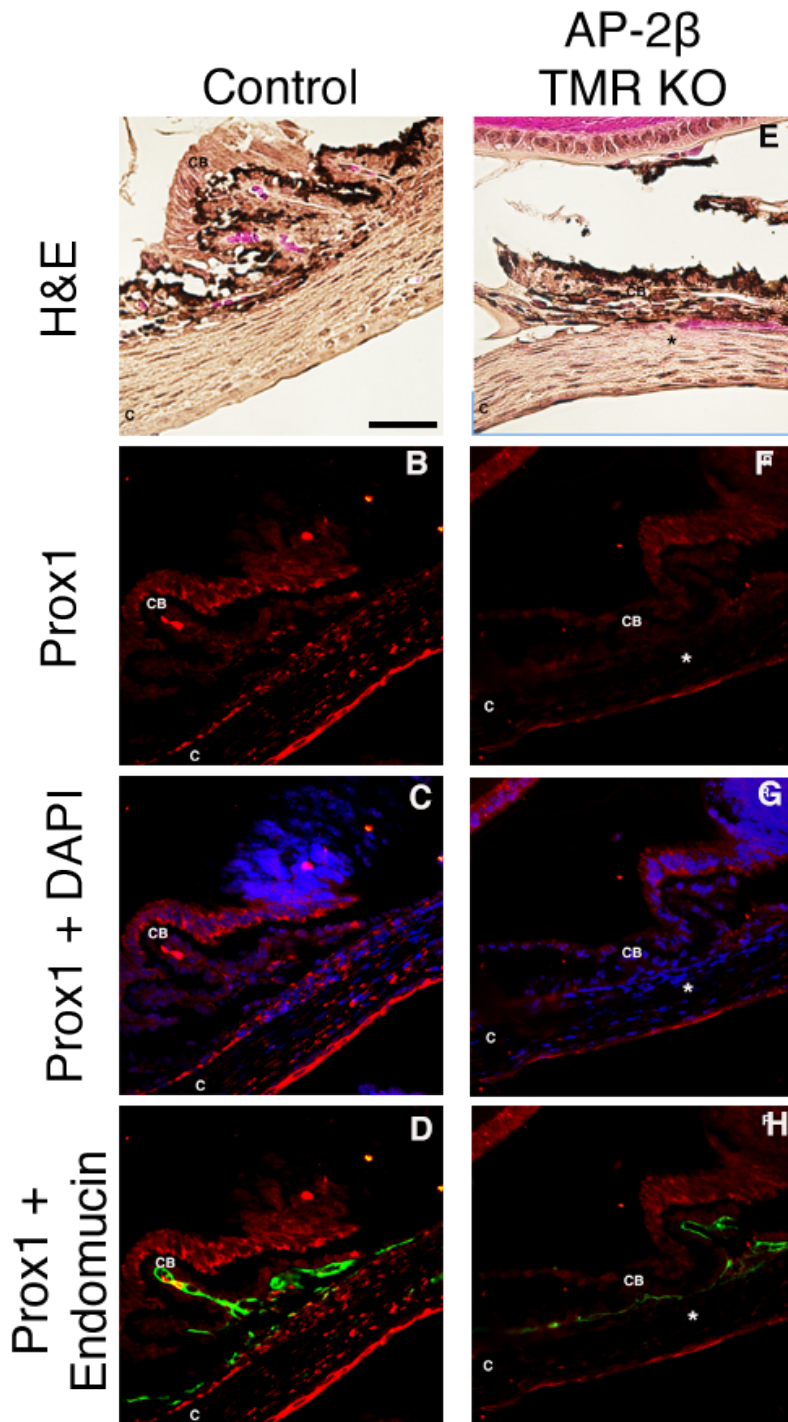
Figure 11. Comparison of SC status and expression of Prox 1 and endomucin between control and AP-2β TMR KO mice at P4. SC is not visibly present in the control (A) or mutant (E) at P4 but expression of nuclear Prox1 in SC region is present in the control (B-D) and absent in the mutant (F-H– asterisks). CB, ciliary body; C, cornea. Scale bar represents 100 μm. Images were acquired using a 40x objective lens.
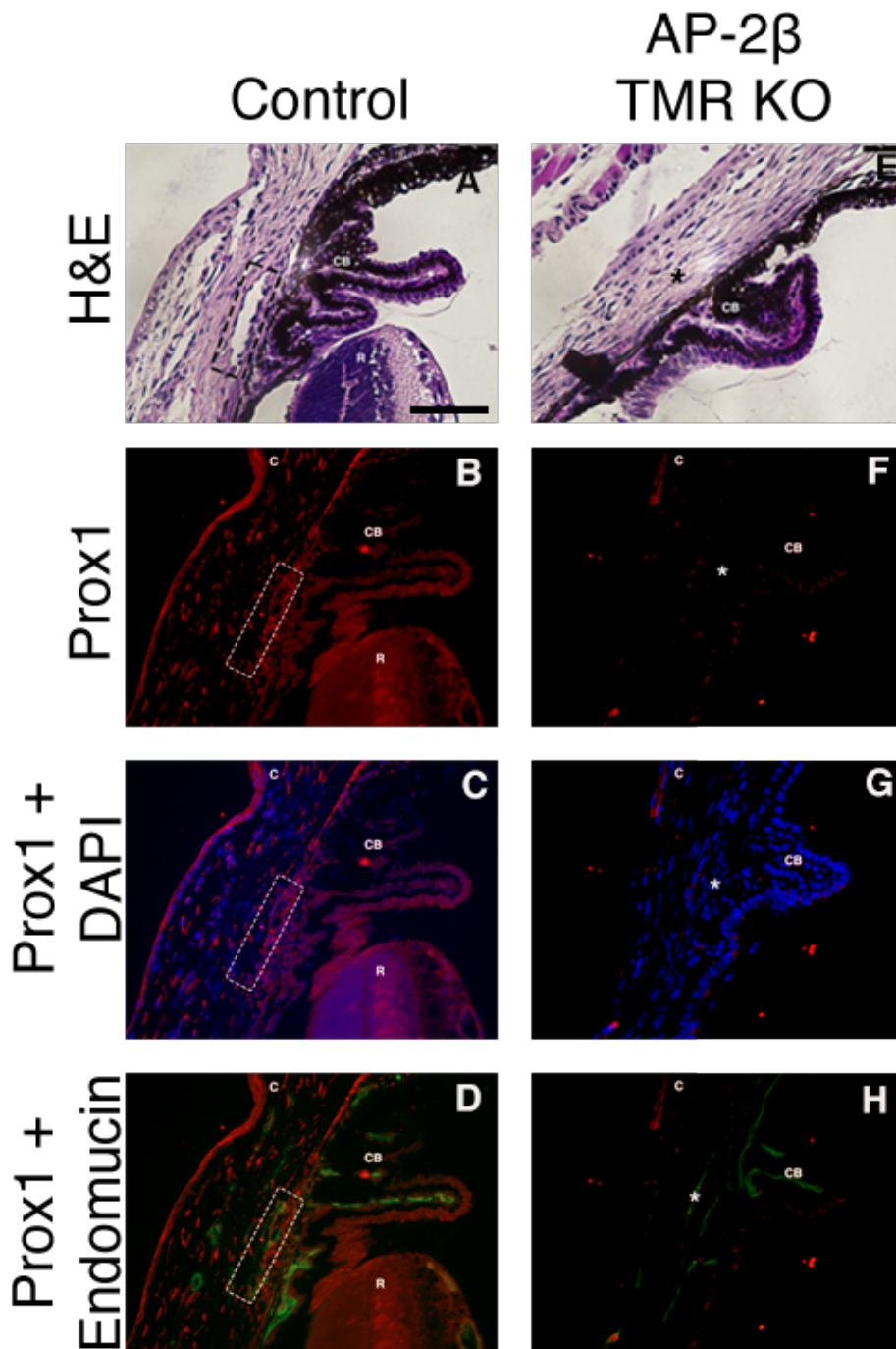
Figure 12. Comparison of SC status and expression of Prox 1 and endomucin between control and AP-2β TMR KO mice at P10. SC is now visibly present in the control (A– rectangle) but absent in the mutant (E– asterisk) at P10. Expression of nuclear Prox1 in SC region is present in the control (B-D– rectangles) but completely absent in the mutant (F-H– asterisks). CB, ciliary body; C, cornea. Scale bar represents 100 μm. Images were acquired using a 40x objective lens.
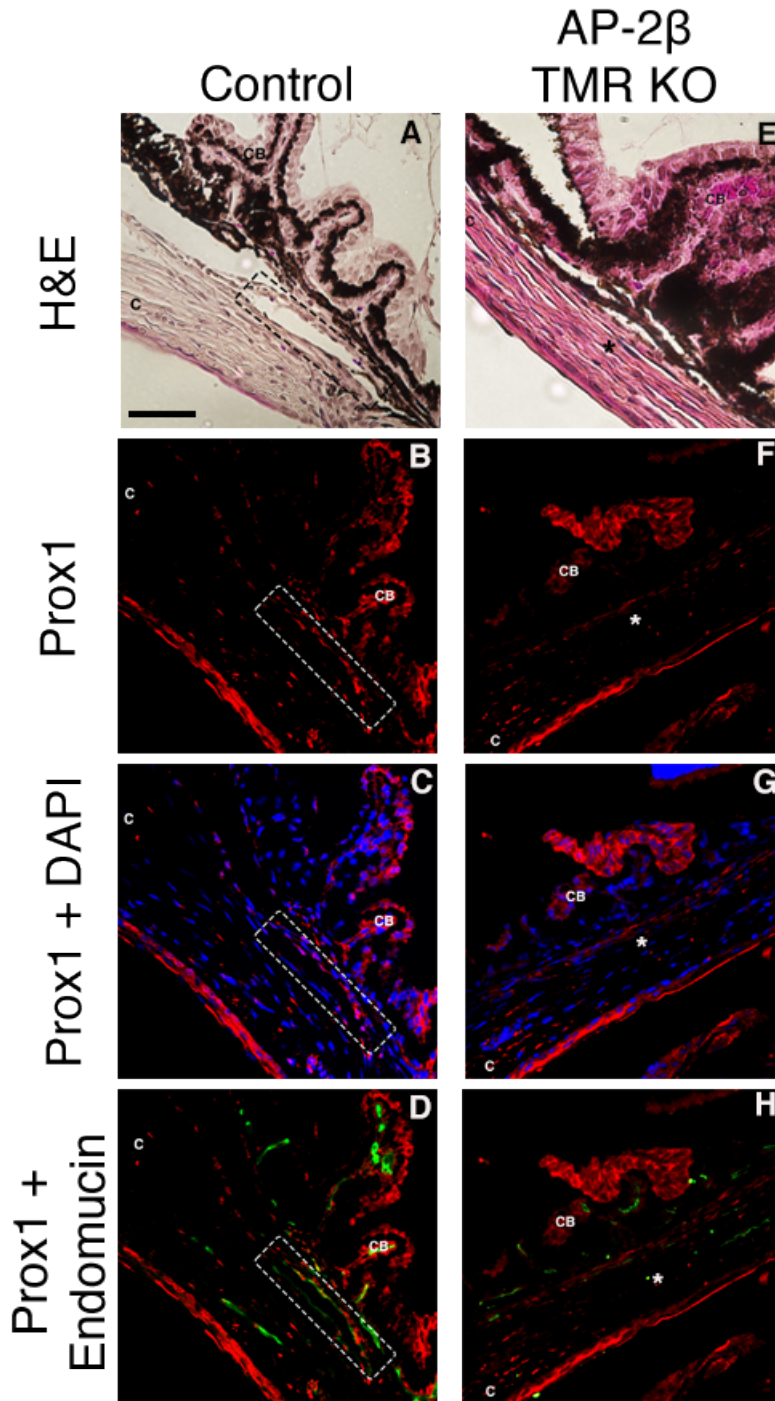
Figure 13. Comparison of SC status and expression of Prox 1 and endomucin between control and AP-2β TMR KO mice at P14. SC is more prominent in the control (A– rectangle) but remains absent in the mutant (E– asterisk) at P14. Expression of nuclear Prox1 in SC region is present in the control, primarily in the inner wall, (B-D– rectangles) but completely absent in the mutant (F-H– asterisks). CB, ciliary body; C, cornea. Scale bar represents 100 μm. Images were acquired using a 40x objective lens.

In addition to Prox1, the expression of another key SC developmental marker, Klf4, was examined at similar time-points. At P4 (n=4 eyes), there was no Klf4 expression observed in the approximate SC region of either wildtype or mutant (Figure 14). By P10 (n=4 eyes), however, nuclear Klf4 was detected in both the inner and outer SC walls of the wildtype, while the same staining pattern was absent in the mutant (Figure 15). At P14 (n=4 eyes), a more elongated SC structure was seen in the wildtype, similar to the H&E stain in Figure 13, and nuclear Klf4 expression was primarily detected in the inner SC wall; once again, this staining was absent in the mutant (Figure 16).
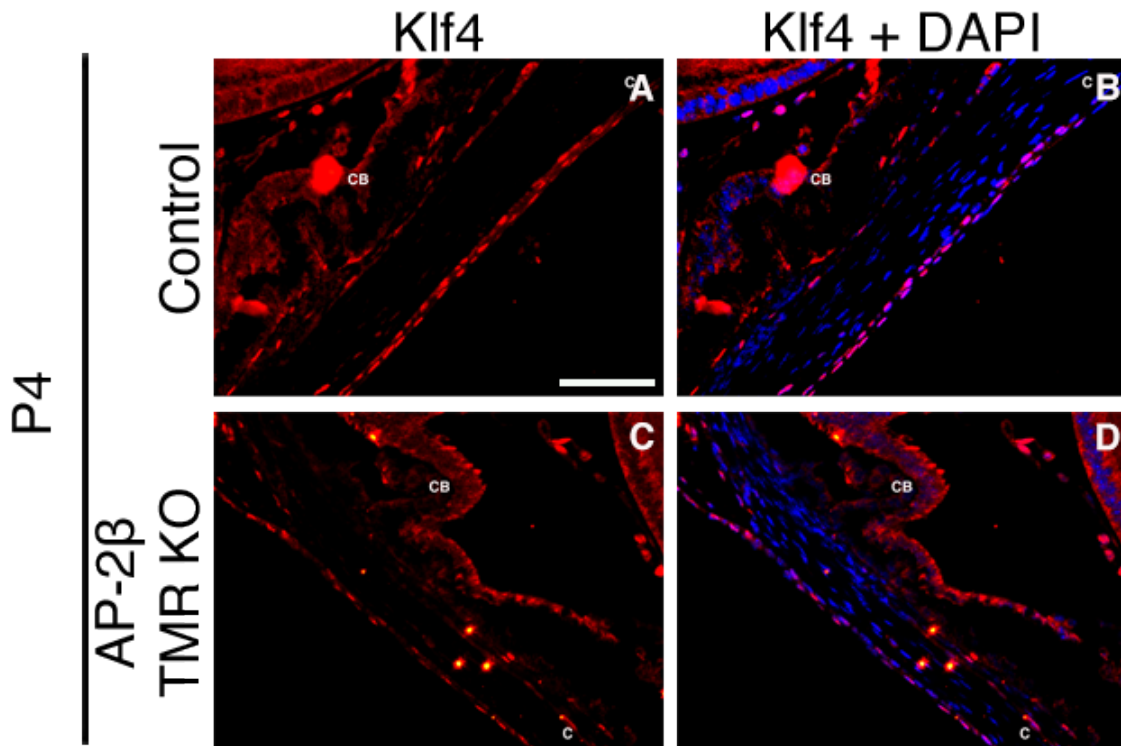
Figure 14. Comparison of expression of Klf4 between control and AP-2β TMR KO mice at P4. Klf4 nuclear expression is absent in both the control and the mutant at P4, as can be seen through overlay with DAPI. CB, ciliary body; C, cornea. Scale bar represents 100 μm. Images were acquired using a 40x objective lens.
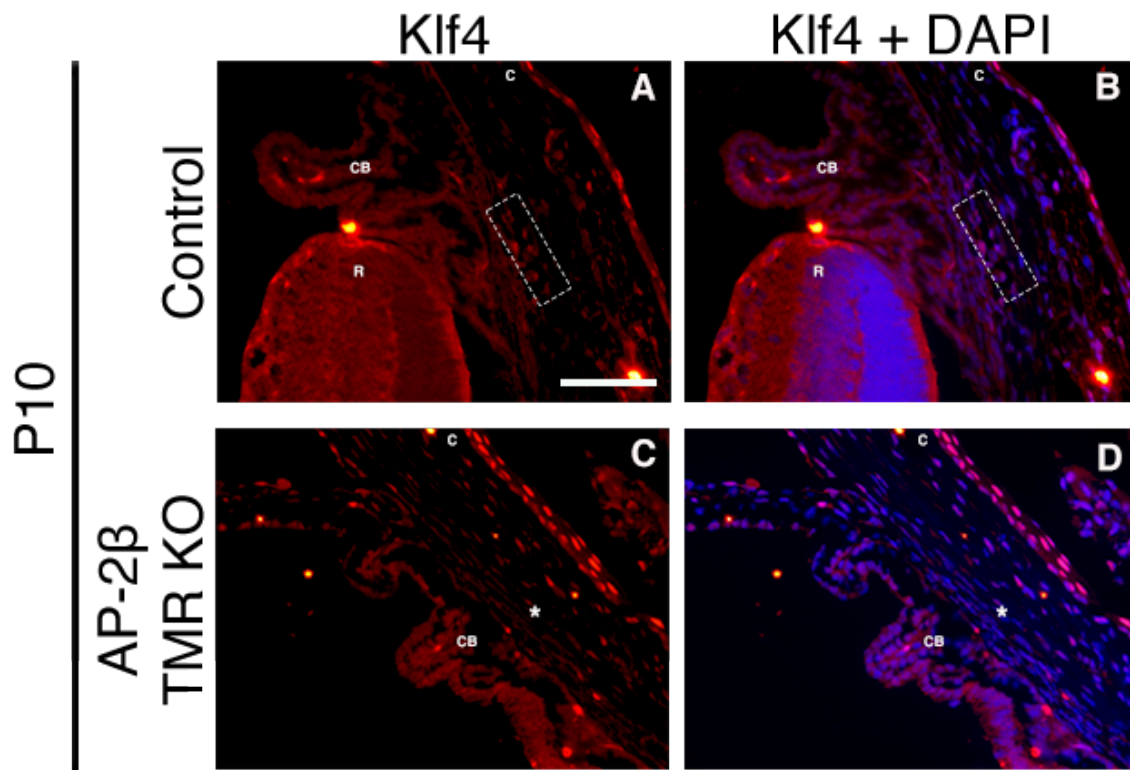
Figure 15. Comparison of expression of Klf4 between control and AP-2β TMR KO mice at P10. Klf4 nuclear expression is present in the control (A-B– rectangles) but not the mutant at P10 (C-D– asterisks). CB, ciliary body; C, cornea; R, retina. Scale bar represents 100 μm. Images were acquired using a 40x objective lens.

Figure 16. Comparison of expression of Klf4 between control and AP-2β TMR KO mice at P14. Klf4 nuclear expression is present in the control (A-B– rectangles) but not the mutant at P10 (C-D– asterisks). CB, ciliary body; C, cornea. Scale bar represents 100 μm. Images were acquired using a 40x objective lens.

4.1.2. Investigating gene expression patterns of key SC markers through HiPlex RNAscope assay

In addition to visualizing the expression of key markers of SC through immunohistochemistry, optimization of a protocol for a HiPlex RNAscope assay has been underway in our lab. This newly developed *in situ* hybridization technique allows for the detection of multiple genes at a single-molecule level in individual cells, while combatting the problem of low RNA stability in traditional *in situ* methods. Due to the fragility of frozen ocular sections, several control studies have been conducted trials to devise a protocol that allows for intact tissue morphology as well as optimal staining. The newly developed protocol has been applied to P4 (n=2 eyes) and P10 (n=2 eyes) wildtype and AP-2β TMR-KO frozen ocular sections and revealed changes in the expression of several genes important for SC development including *Prox1*, *Klf4*, *Angpt1*, and *Tie2*. At both P4 and P10, positive RNA signal for *Prox1* was observed in the wildtype eye in the approximate SC region in the form of small bright dots, with the same positive signal greatly reduced in AP-2β TMR KO eyes (see rectangles– Figure 17; top panels depict fluorescent images and bottom panels show fluorescence with brightfield). On the other hand, for *Klf4*, no signal was observed in the approximate SC region in either wildtype of mutant eyes at P4 (see rectangles– Figure 18A; top panels depict fluorescent images and bottom panels show fluorescence with brightfield). By P10, however, positive signal was detected in the wildtype while expression remained absent in the mutant (see rectangles– Figure 18B; top panels depict fluorescent images and bottom panels show fluorescence with brightfield). The assay also assessed the gene expression of *Tie2* and *Angpt1*, both of

which comprise a receptor-ligand system that has been shown to be critical for development of SC (Thomson et al., 2017). The gene expression of *Tie2* presented similarly to *Prox1*, with positive signal in the approximate SC region observed only in the wildtype eye at both P4 and P10 (see rectangles– Figure 19; top panels depict fluorescent images and bottom panels show fluorescence with brightfield). Gene expression of *Angpt1* was also investigated, specifically in the trabecular meshwork region. Positive signal was detected in the trabecular meshwork region of wildtype eyes at both P4 and P10, yet remained absent in the mutant at both stages (see rectangles– Figure 20; top panels depict fluorescent images and bottom panels show fluorescence with brightfield).

Figure 17. Prox1 gene expression in control and AP-2β TMR KO at P4 and P10. *(A-B)* Prox1 gene expression is present in the control at both P4 and P10, but is absent in AP-2β TMR KO eyes in the approximate SC region (rectangles). CB, ciliary body; C, cornea; R, retina. Scale bar represents 100 μm. Images were acquired using a 40x objective lens.
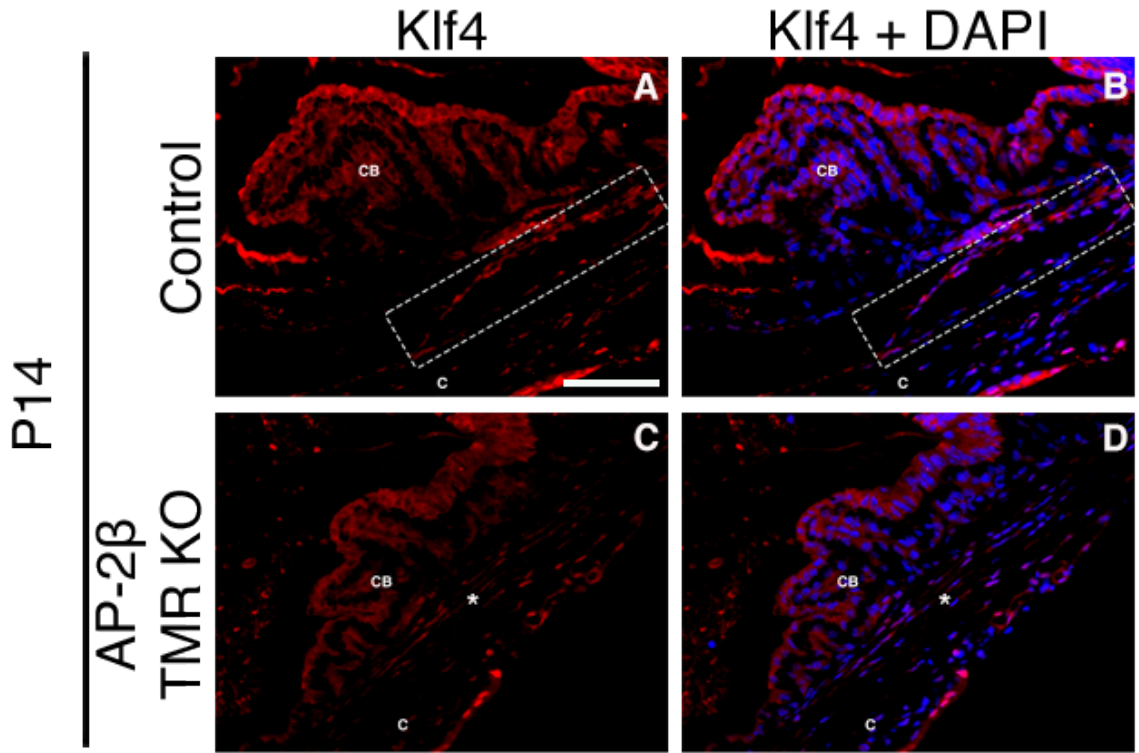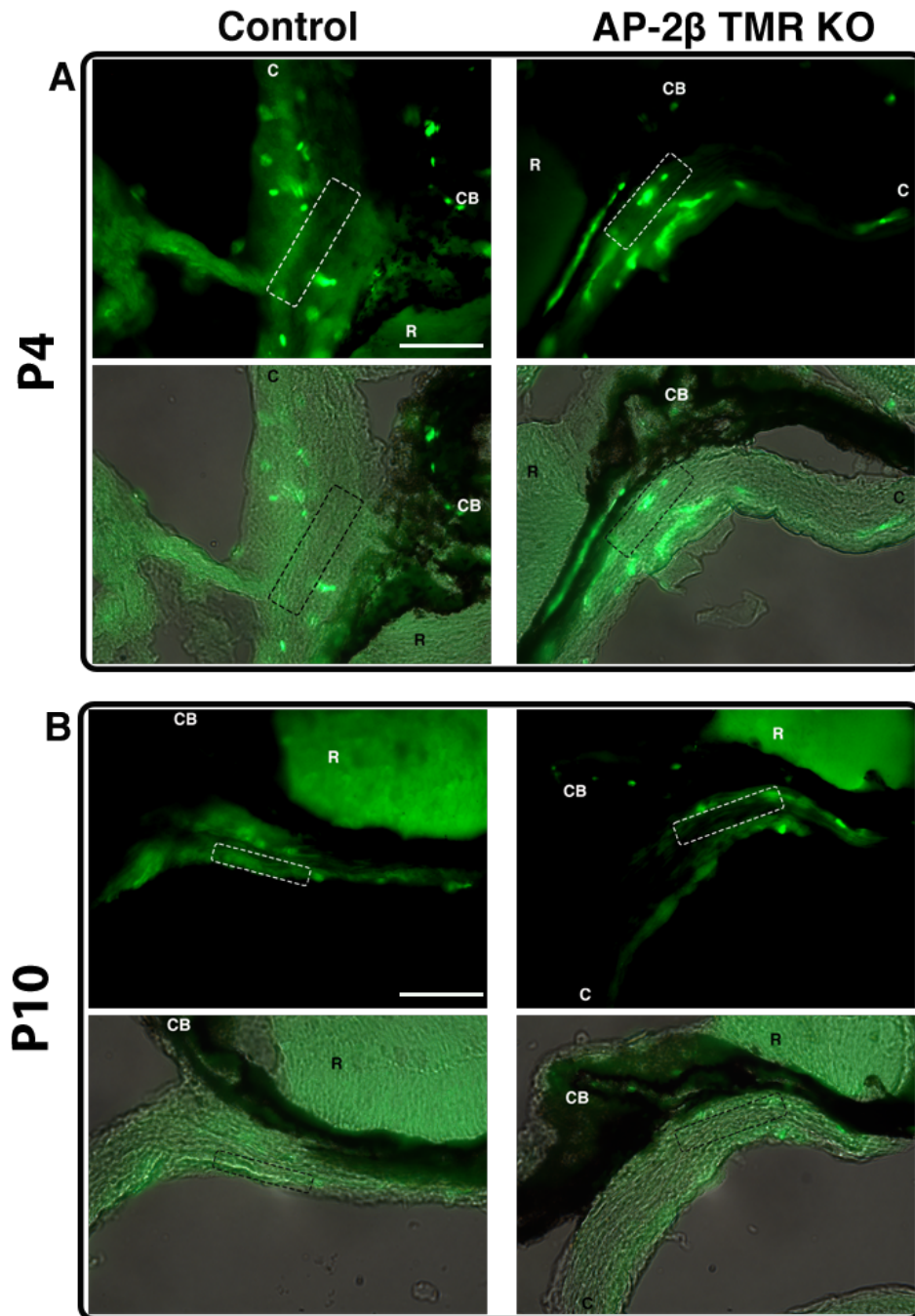
Figure 18. Klf4 gene expression in control and AP-2β TMR KO at P4 and P10. *(A)* Klf4 gene expression is absent from both control and AP-2β TMR KO eyes in the approximate SC region at P4 (rectangles). *(B)* Positive RNA signal for Klf4 is detected in the control at P10 but remains absent in the mutant in the approximate SC area (rectangles). CB, ciliary body; C, cornea; R, retina. Scale bar represents 100 μm. Images were acquired using a 40x objective lens.
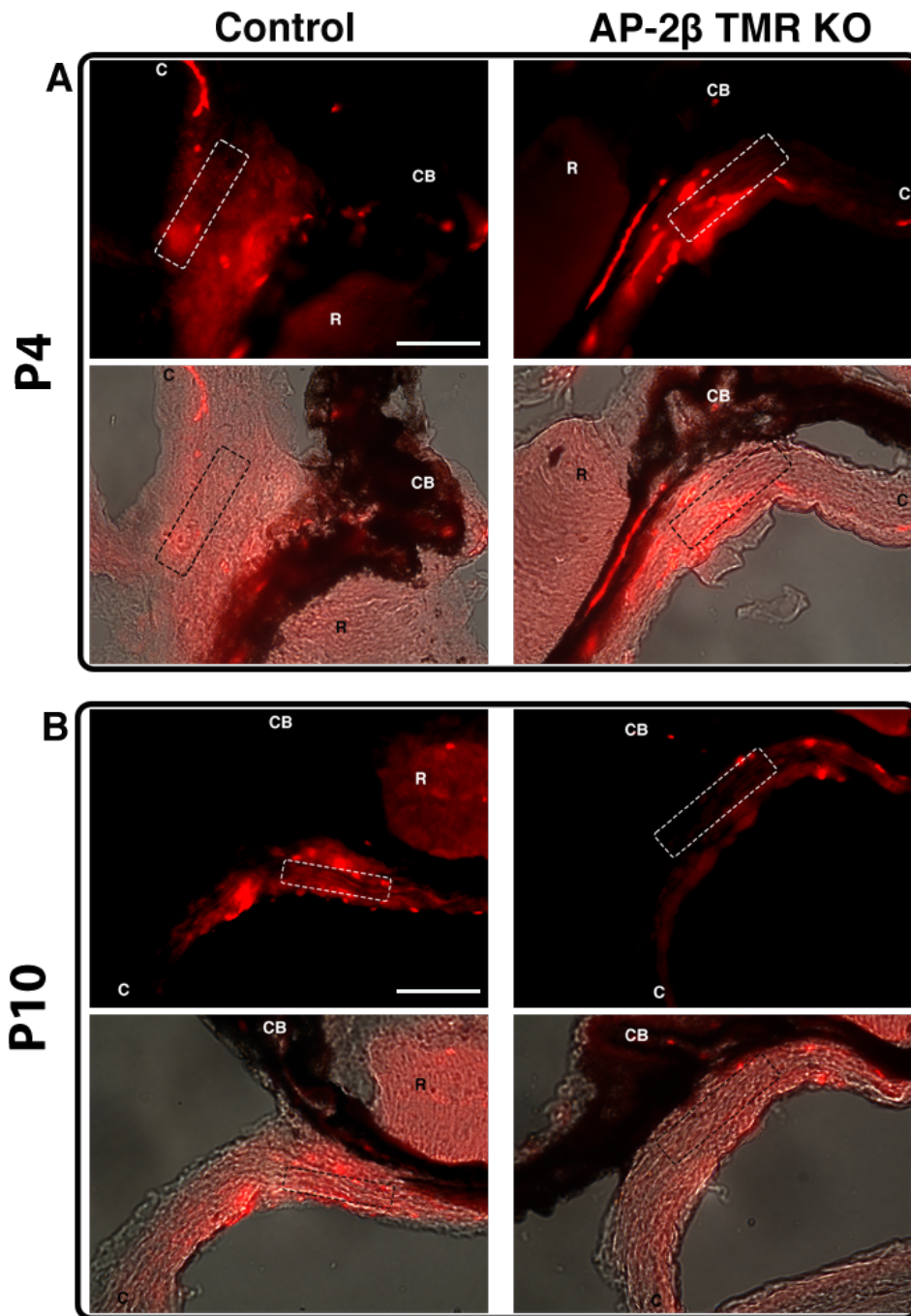
Figure 19. Tie2 gene expression in control and AP-2β TMR KO at P4 and P10. *(A-B)* Tie2 gene expression is present in the control at both P4 and P10 but is absent in AP-2β TMR KO eyes in the approximate SC region (rectangles). CB, ciliary body; C, cornea; R, retina. Scale bar represents 100 μm. Images were acquired using a 40x objective lens.
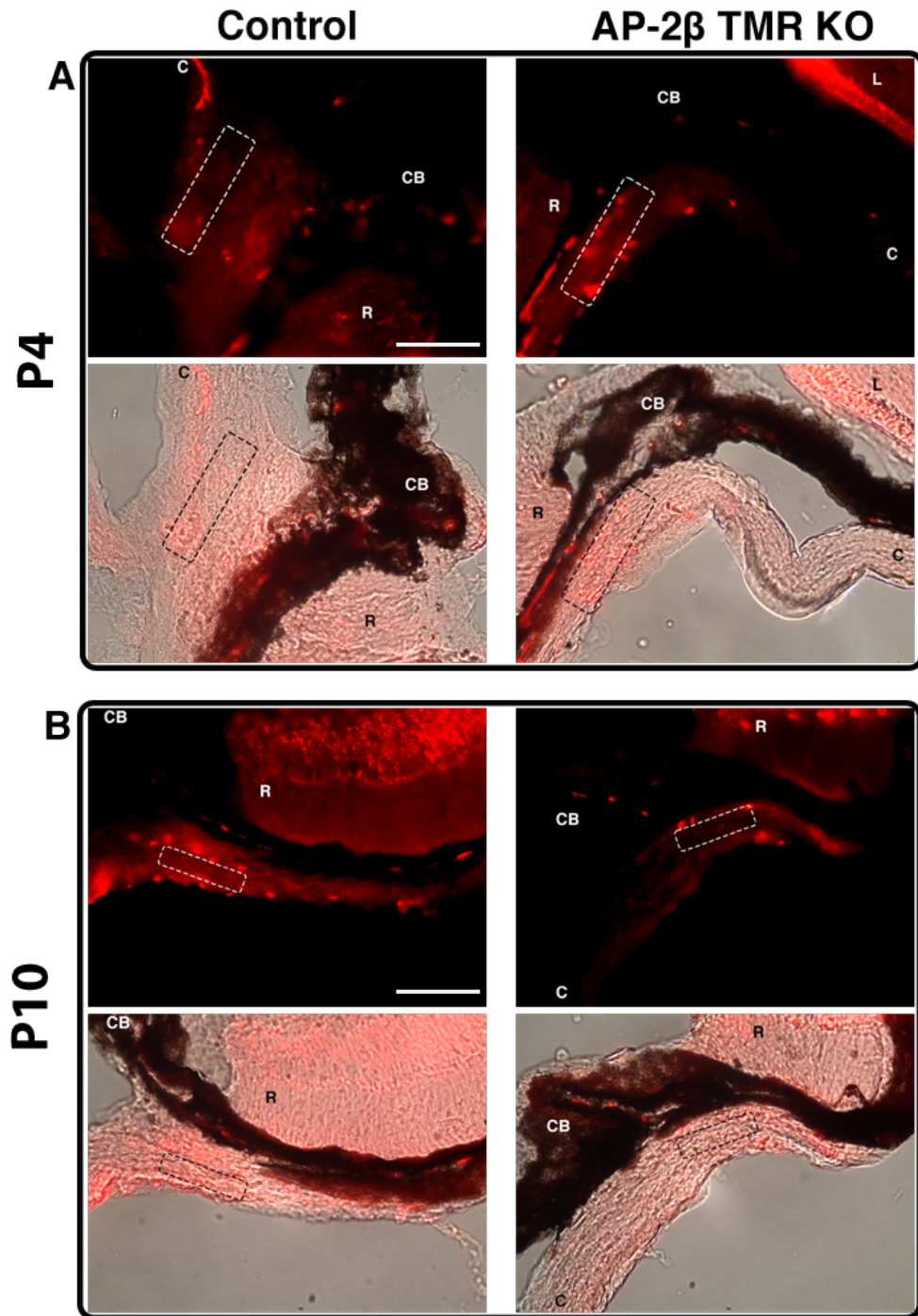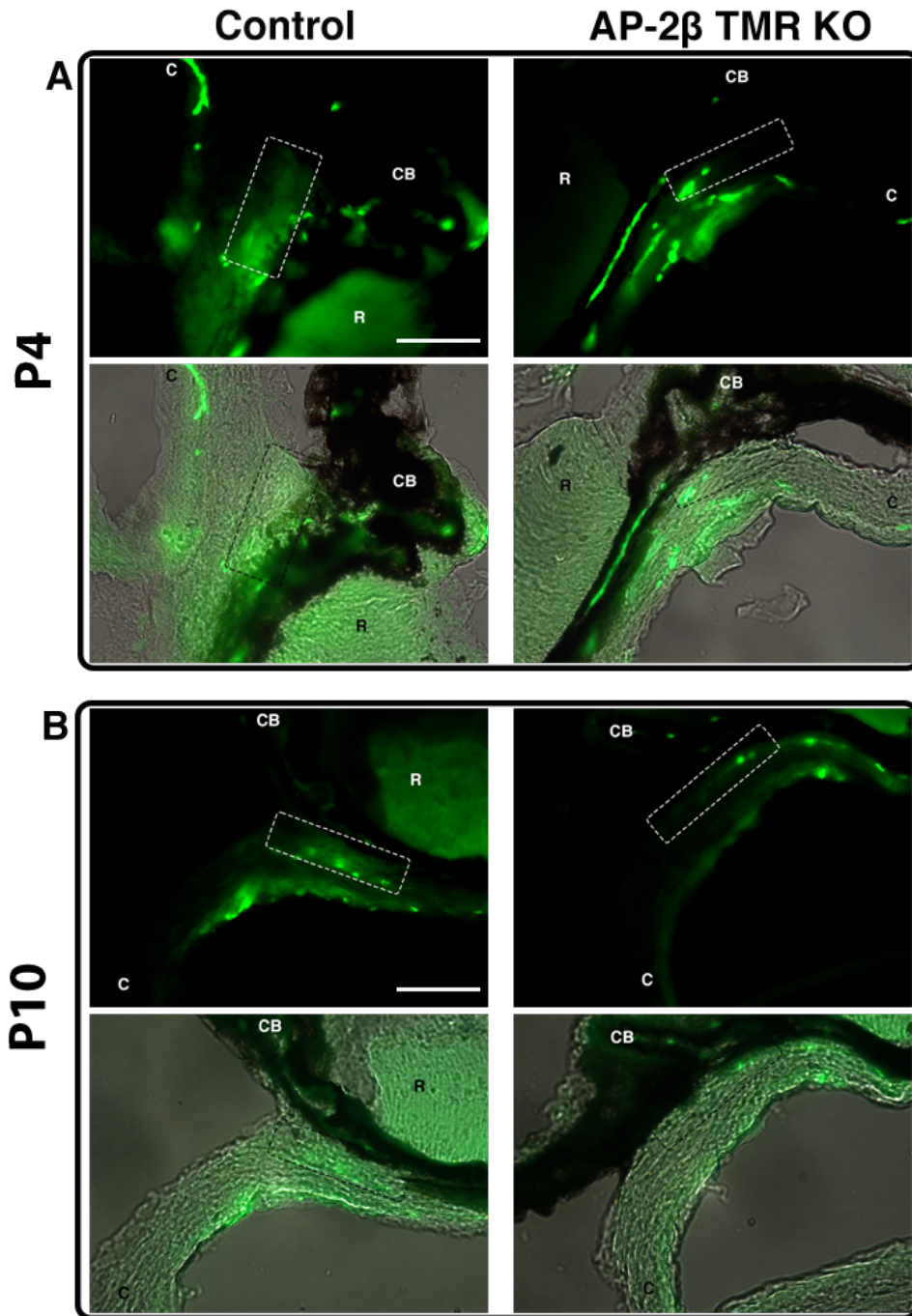
Figure 20. Angpt1 gene expression in control and AP-2β TMR KO at P4 and P10. *(A-B)* Angpt1 gene expression is present in the control at both P4 and P10 but is absent in AP-2β TMR KO eyes in the approximate trabecular meshwork region (rectangles). CB, ciliary body; C, cornea; R, retina. Scale bar represents 100 μm. Images were acquired using a 40x objective lens.

4.2. Aim 2: Assess the functionality of the uveoscleral outflow pathway in the AP-2β TMR-KO mice and determine if it is being used to reduce IOP.

4.2.1. Investigating functionality of uveoscleral outflow in AP-2β TMR-KO eyes using a dextran tracer

We have demonstrated previously that the AP-2β TMR-KO mutants exhibit elevated IOP when compared to wildtypes, which can be reduced temporarily through treatment with latanaprost, a prostaglandin analog (Figure 9) (Taiyab et al., 2022). Since the conventional outflow pathway is blocked in the AP-2β TMR-KO mutants, it is expected that the reduction in IOP may be due to increased outflow through the uveoscleral pathway after latanaprost treatment. I aimed to further investigate aqueous humor outflow and the functionality of the uveoscleral pathway in the mutants through injection of a 40 kDA dextran tracer (Lindsey & Weinreb, 2002).

Injections with PBS and dextran were carried out in both wildtype and mutant eyes from the following groups: untreated (n=5 eyes), treated with latanaprost for 5 minutes (n=5 eyes), and treated with latanaprost for 10 minutes (n=5 eyes). In untreated wildtype eyes, the dextran was present in the ciliary processes, the trabecular meshwork and SC region, and the choroid, suggesting outflow through both the conventional and the uveoscleral pathway (Figure 21A). In the AP-2β TMR-KO mutant eyes, however, the dextran particles were observed to be clustered in the anterior chamber with minimal amounts of tracer present in the outflow pathways (Figure 21D). 5 minutes after treatment with latanaprost, a similar outflow pattern was observed in the wildtype as the untreated group (Figure 21B). In the mutant, however, dextran was now detected in regions

associated with the uveoscleral pathway, including the supraciliary and suprachoroidal spaces, instead of clustered in the anterior chamber (Figure 21E). 10 minutes after latanaprost treatment, the dextran was mostly cleared out from the control and detected further along the uveoscleral pathway in the mutant (Figure 21C, F).

Additionally, the corrected total fluorescence was calculated and analyzed for the injected eyes in two different regions: the central anterior chamber and the region of the outflow pathways. In the anterior chamber, the fluorescence was extremely low and not significantly different for any group except the untreated mutant, for which the fluorescence was significantly greater than all others ($P \leq 0.01$) (Figure 22). On the other hand, in the region of the outflow pathways, the fluorescence was significantly different when comparing the untreated control and mutant ($P \leq 0.05$), as well as the untreated mutant with the 5 minutes and 10 minutes post-latanaprost treated mutants ($P \leq 0.01$ and $P \leq 0.001$ respectively) (Figure 23).
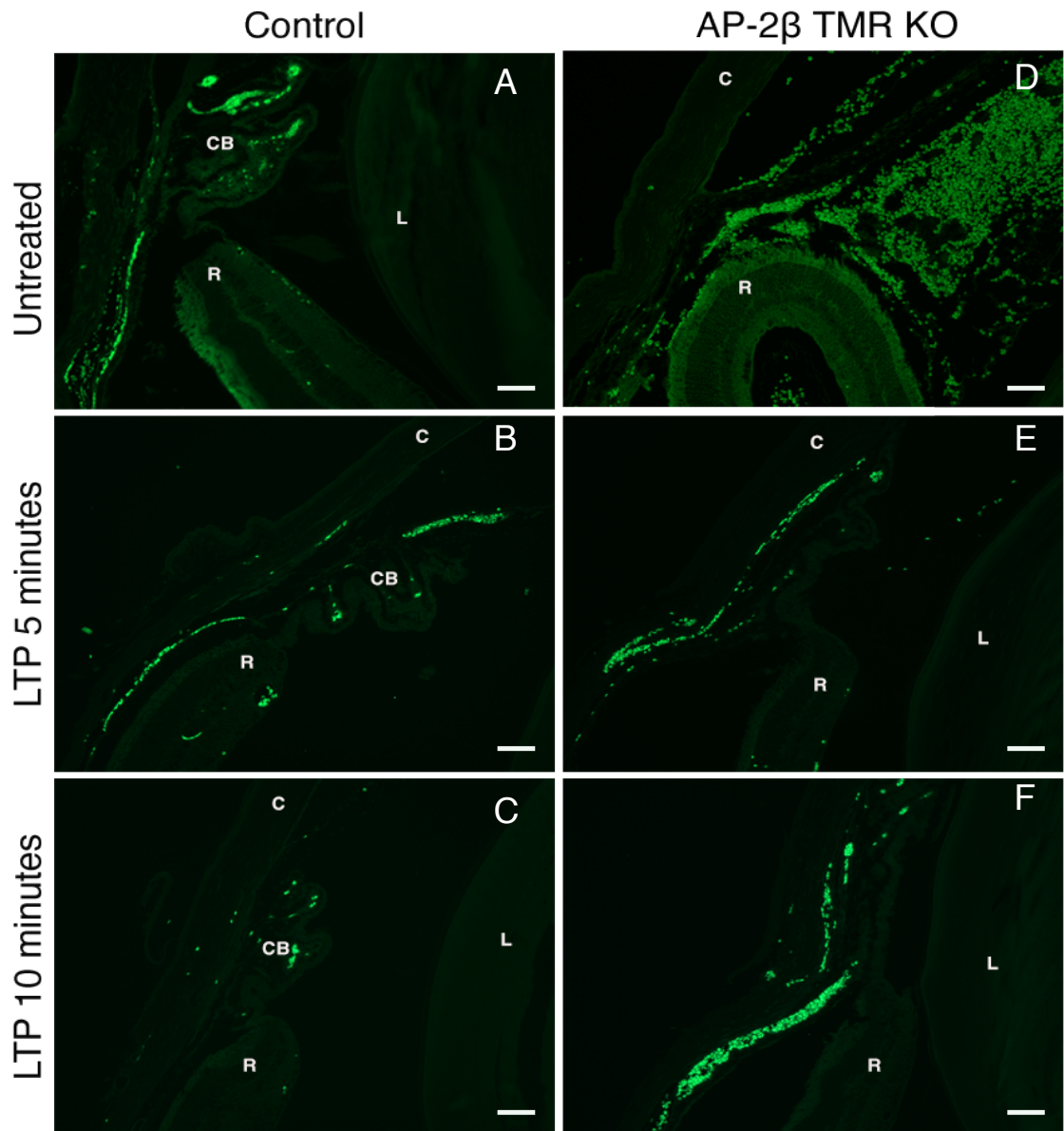
Figure 21. Aqueous humor outflow of control and AP-2β TMR-KO adult mice, compared prior to, 5 minutes after, and 10 minutes after latanaprost treatment. (*A, D*) In the untreated control, outflow is seen through both the conventional and uveoscleral pathways as the dextran is seen in the trabecular meshwork and SC region, the ciliary processes, and the choroid. In the untreated mutant, dextran is clustered in the anterior chamber. *(B, E)* 5 minutes after latanaprost treatment, dextran continues to flow out normally in the control, but now is also seen in regions of the uveoscleral pathway in the mutant. *(C, F)* 10 minutes after latanaprost treatment, dextran is mostly cleared out from the control and is detected further along the uveoscleral pathway in the mutant. C, cornea; L, lens; R, retina; CB, ciliary body. Scale bars represent 100 μm. Images were acquired using a 20x objective lens.
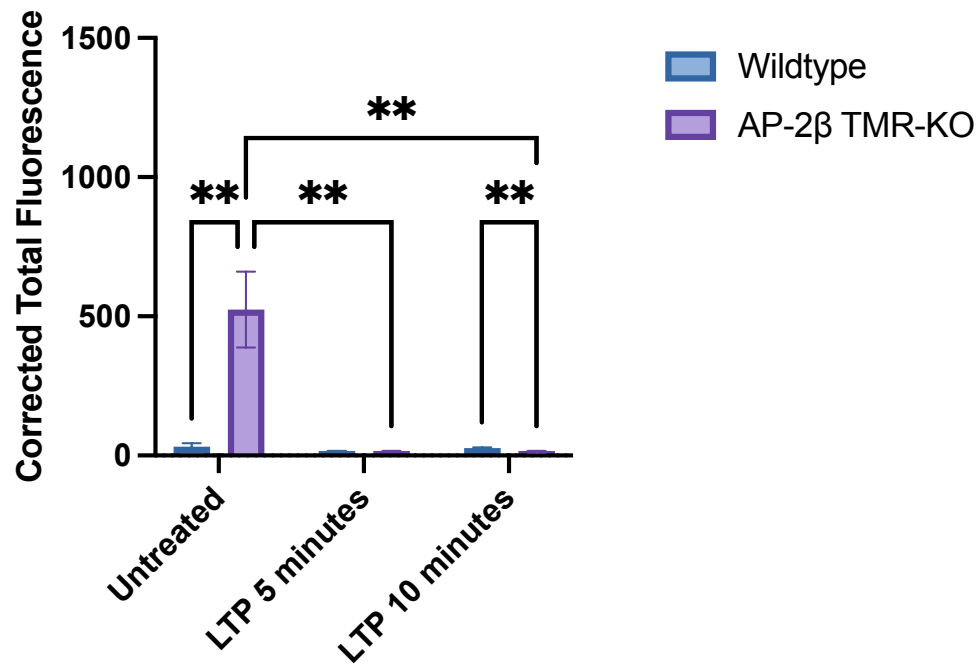
Figure 22. Corrected total fluorescence of injected dextran in the anterior chamber of untreated and latanaprost treated wildtype and AP-2β TMR-KO adult mice. Fluorescence of dextran tracer in the anterior chamber is low and not significant for any group except the untreated mutant. The untreated mutant exhibits significantly higher fluorescence in the anterior chamber when compared to the untreated control ($P \leq 0.01$) as well as the 5 minutes and 10 minutes post latanaprost treated mutant ($P \leq 0.01$ for both). LTP, latanaprost.
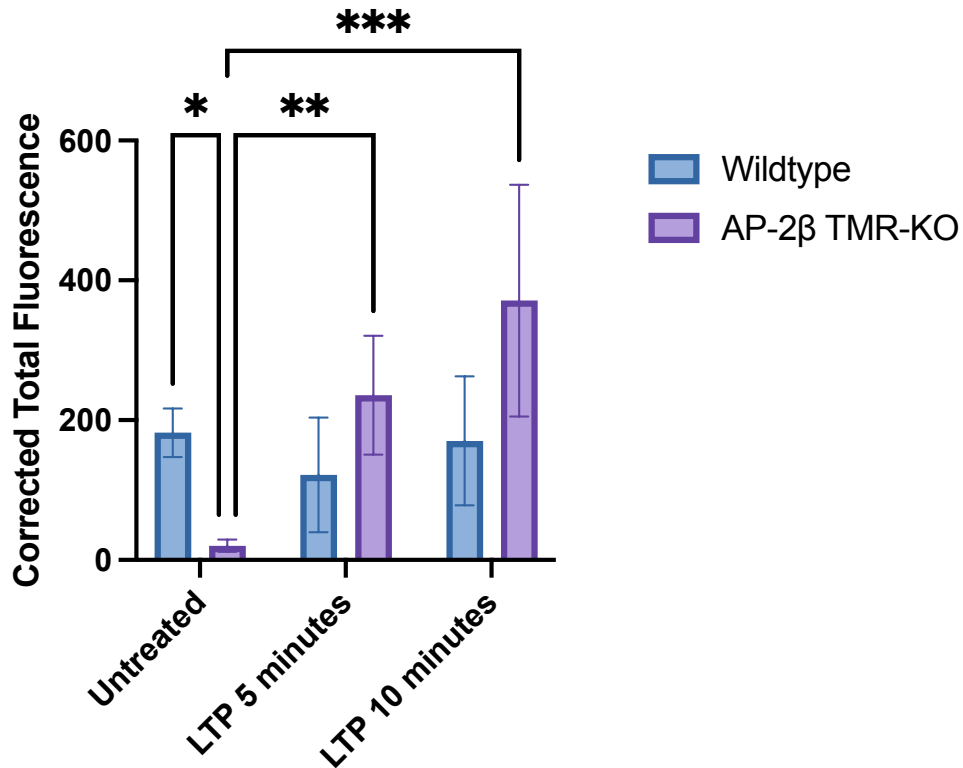
Figure 23. Corrected total fluorescence of injected dextran in the region of the outflow pathways of untreated and latanaprost treated wildtype and AP-2β TMR-KO adult mice. Fluorescence of dextran tracer in the region of the outflow pathways is significantly higher in the untreated control compared to the untreated mutant ($P \leq 0.05$), and in the 5 minutes and 10 minutes treated mutants compared to the untreated mutant ($P \leq 0.01$ and $P \leq 0.001$, respectively). LTP, latanaprost.

An additional experiment was performed to confirm that the intracameral injections did not have any effect on IOP. Control (n = 6 eyes) and AP-2β TMR KO (n = 6 eyes) mice were intracamerally injected with the dextran tracer and subsequently treated with latanaprost. IOP measurements were taken 10 minutes after latanaprost treatment. As is evident in Figure 24, the trends in IOP prior to and after latanaprost treatment remain the same as we have previously demonstrated, confirming that the dextran injection did not affect IOP measurements (Taiyab et al., 2022).
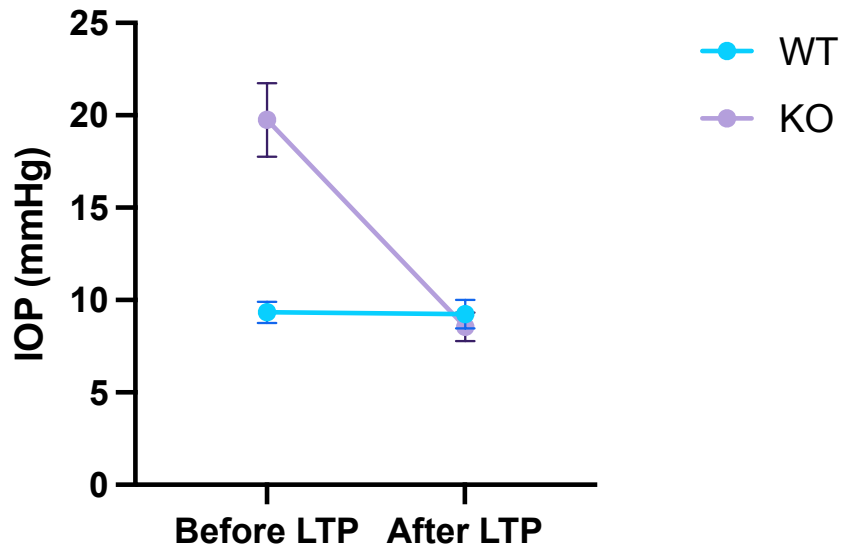
Figure 24. IOP measurements before and after latanaprost treatment of adult control vs. AP-2β TMR KO mice injected with dextran tracer. IOP of control mice (n = 6 eyes) does not change upon LTP treatment. IOP of mutant mice (n = 6 eyes) shows a significant reduction in IOP (P ≤ 0.0001) after LTP treatment.

CHAPTER 5

DISCUSSION, FUTURE DIRECTIONS, AND CONCLUSION

Glaucoma is a multifactorial disease characterized by damage to the optic nerve due to elevated IOP, which occurs as a result of an imbalance between aqueous humor production and drainage (Kass et al., 2002). IOP is maintained by secretion of aqueous humor from the ciliary body, which exits the eye through the drainage structures at the iridocorneal angle, such as the trabecular meshwork and SC (Machiele et al., 2020). Prior research suggests that developmental glaucomas result from defects in the patterning, migration, and/or differentiation of the POM cell population (Williams & Bohnsack, 2015). The POM is derived from the NCC population and the paraxial mesoderm cell population (Gage et al., 2005). The NCC population is known to contribute to the development of the corneal endothelium and stroma, ciliary body muscle and stroma, iris stroma, and cells of the aqueous outflow structures including the trabecular meshwork (Williams & Bohnsack, 2015). The paraxial mesoderm cell population is known to contribute to the development of all vascular endothelium, such as SC (Gage et al., 2005). However, the genetic regulation and subsequent signaling cascades that control the development of anterior angle structures that regulate aqueous humor outflow, specifically the trabecular meshwork and SC, remain to be elucidated.

Recently, using a GWAS study, it has been observed that SNPs for the *Tfap2b* locus, the gene that encodes transcription factor AP-2β, may be associated with glaucoma in humans (J. Wiggs, personal communication). Since germline knockout mice for AP-2β died perinatally due to various defects associated with the heart, kidneys, and/or nervous system, we have developed a floxed mouse for deleting AP-2β in specific tissues (Moser, Pscherer, et al., 1997). In order to understand the role of AP-2β in POM-mediated

development of anterior angle structures, we have deleted AP-2β from the developing POM by using a novel MgpCre recombinase system that expresses Cre-recombinase under control of the Mgp promoter, and its expression is confined to the POM of the developing mouse eye (MgpCre mice were obtained from our collaborator, Dr. Terete Borras) (Borras et al., 2015). The mutant mice show an absence of the trabecular meshwork and an underdeveloped SC, the main tissues that contribute to the conventional outflow pathway, resulting in increased IOP which can be temporarily reduced through latanaprost treatment (Figures 8, 9) (Taiyab et al., 2022). This model was the basis of all experiments conducted in this project.

5.1. Effect of AP-2β deletion on SC development

By examining the expression of key SC markers after AP-2β deletion from the POM, we were able to gather a better understanding of the genes that regulate development of the structure as well as gain insight into the role of AP-2β in anterior segment development. It has been established previously that Prox1 expression begins in the SC region around P4, and continues being expressed in adulthood. However, by P10 the diminished expression in the outer wall relative to the inner wall is evident (Kizhatil et al., 2014). This is consistent with the immunohistochemical stain we performed for Prox1 in the wildtype. Expression is detected in the SC region at P4 in the wildtype but absent in the mutant, and remains this way for all stages examined (i.e. P7, P10, P14, P30) (Figures 11-13). At P10, expression is much greater in the inner wall compared to the outer wall and by P14, expression is mostly only detected in the inner wall (Figres 12-13). This suggests that while Prox1 may be required in the approximate SC region early in the structure's

developmental timeline, the protein is eventually selectively expressed by cells of the inner wall. Prox1 has been deemed the master regulator of lymphatic fate as it promotes the transition to LECs from BECs, and is required for the maintenance of lymphatic identity (Park et al., 2014). There has been debate about the identity of SC, where some studies propose it is similar to vascular endothelium but others argue it is a lymphatic vessel; in recent years it has been put forth that the structure is blood vascular in origin and later acquires lymphatic fate through the upregulation of Prox1 (Foets et al., 1992; Hagerling et al., 2013; Hamanaka et al., 1992; Park et al., 2014; Truong et al., 2014). The staining pattern observed in the immunohistochemistry results, however, may suggest that parts of SC transition to a lymphatic identity, such as the inner wall, while others, like the outer wall, retain their vascular origin. A potential explanation for this could be the location of the inner wall, adjacent to the JCT of the trabecular meshwork, through which aqueous humor is filtered and propelled into SC (Ethier et al., 2004). The pressure on SC caused by the aqueous humor flow may be the reason for Prox1 upregulation in the approximate region, before the tubular structure has formed and the inner and outer walls have separated; this is supported by the fact that the start of aqueous flow and the expression of Prox1 have been shown to coincide at approximately P4 (Figure 25) (Kim et al., 2017). Later, when the tubular structure is more defined, Prox1 may then selectively be expressed by the inner wall. If this is in fact the case, then lack of aqueous humor flow in the AP-2β TMR-KO mice may be the reason for absence of Prox1 expression. We have previously shown with this model that AP-2β plays a cell-autonomous role in the development of the trabecular meshwork, and its deletion from the POM leads to the absence of the region, thus restricting

aqueous flow through the conventional pathway (Taiyab et al., 2022). Additionally, we

also examined the gene expression of *Prox1* using a HiPlex RNAscope assay, in
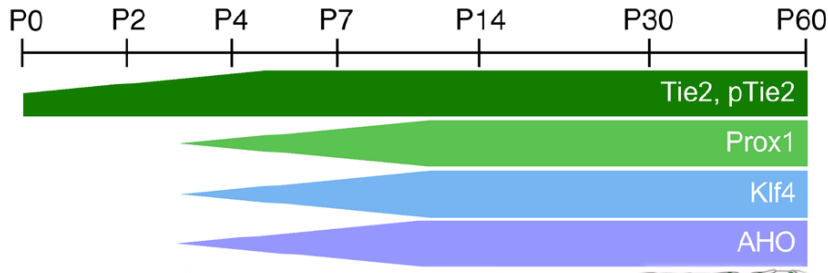
Figure 25. Temporal changes in Tie2, pTie2, Prox1, and Klf4 expression in Schlemm's canal, and gain of predicted aqueous humor outflow. Expression of Tie1 and pTie2 beings embryonically and continues past P60. Expression of Prox1 and Klf4, as well as gain of predicted aqueous humor outflow (AHO) begins at P4 and continues past P60. Adapted from (Kim et al., 2017).

conjunction with several other genes. Similar to the immunohistochemical stain for Prox1,

expression in the wildtype eyes was observed at both P4 and P10 in the SC region, whereas

it was absent in the mutants (see rectangles– Figure 17). Interestingly, the RNA signal for

Prox1 at P4 was more spread out in the entire region, even outside the area marked by the

rectangle, whereas by P10 it was specifically present only in the area marked by the

rectangle. It is difficult to compare the signal in the inner and outer walls with this assay

due to the background fluorescence. However, the more specific staining pattern may be

consistent with the conclusions drawn from the immunohistochemistry results.

Another marker investigated was Klf4, a transcription factor which has been shown

to respond to shear stress in other systems (McCormick et al., 2001). Previous reports have

proposed that Klf4 may work cooperatively with Prox1 in SC development as it was shown

that initiation of flow in BECs recruited Klf4 to a recognized enhancer sequence in the first

intron of Prox1. However, this was not sufficient by itself to turn on Prox1 expression (Park

et al., 2014). We performed immunohistochemical staining for Klf4 in wildtype and AP-

2β TMR-KO at the same time-points as Prox1. At P4, Klf staining was absent in both the wildtype and AP-2β TMR-KO eyes (Figure 14). By P10, a small tube-like structure was visible in the wildtype with positive staining in both the inner and outer walls, but this staining was absent in the mutant (see rectangles and asterisks– Figure 15). At P14, a similar pattern of staining was seen as Prox1, with Klf4 expression primarily present in the inner SC wall relative to the outer in the wildtype, while remaining absent in the mutant (see rectangles and asterisks– Figure 16). This similar pattern provides support for the theory that Prox1 and Klf4 work cooperatively in regulating SC development. Additionally, the increased presence of shear stress responsive Klf4 in the cells that experience the most pressure from flow further suggests that absence of this flow in the AP-2β TMR-KO mutants may be hindering its expression. The RNAscope assay performed also examined the gene expression of *Klf4*, in which the RNA signal observed was consistent with the results of the immunohistochemical stain. As can be noted in Figure 18, positive RNA signal for *Klf4* at P4 in the SC region of both wildtype and mutant is absent. The positive staining seen at this stage is in the corneal region, where *Klf4* is known to be expressed in the epithelium (Swamynathan et al., 2008). By P10, positive RNA signal was detected in the wildtype in a similar pattern as *Prox1*, whereas positive signal was absent in the mutant (Figure 18).

Moreover, the RNAscope assay also assessed the gene expression patterns of *Tie2*, a tyrosine receptor kinase important for vascular homeostasis, and *Angpt1*, its primary ligand (Souma et al., 2016). This receptor-ligand system, in addition to other angiopoietins, comprises an endothelial growth factor pathway and it has been previously demonstrated

that Angpt1-Tie2 signaling is necessary for development of SC in mice (Thomson et al., 2017). Angpt1 is expressed in the trabecular meshwork, and studies have proposed that it is secreted by these cells towards SC, the endothelium of which highly expresses Tie2 (Thomson et al., 2021). Angpt1 knockout in the neural crest leads to decreased SC area and increased IOP, highlighting the importance of Angpt1 release by the trabecular meshwork for development of SC (Thomson et al., 2021). In our RNAscope assay, positive RNA signal for *Tie2* was present in the SC region of the wildtype at both P4 and P10, while remaining completely absent in the AP-2β TMR-KO mutants at both stages (see rectangles– Figure 19). *Angpt1* signal was detected in the approximate trabecular meshwork region of the wildtype at both P4 and P10, but was absent in the mutant at both stages (see rectangles– Figure 20). This result points to a disruption in Angpt1-Tie2 signaling by the deletion of AP-2β from the POM, thus hindering SC development. Tie2 expression in SC has been reported as early as P2, earlier than Prox1 and prior to the initiation of aqueous flow, suggesting that its absence in the mutants may be due to an interference in the signaling pathway that normally leads to its expression because of AP-2β deletion (Kim et al., 2017). Specifically, the crosstalk and reciprocal relationship between the trabecular meshwork and SC may be disrupted as the trabecular meshwork fails to develop, which in turn prevents normal development of SC. It is an established fact that the morphological differences between the inner and outer SC walls are due to the location of the inner wall adjacent to the trabecular meshwork. Thus, it is entirely possible that in addition to directing the morphology of SC, the trabecular meshwork also plays a role in regulating its development. Additionally, the lack of aqueous flow in the AP-2β

61

TMR-KO mice could be a secondary effect of the disruption of this crosstalk, which could be preventing the upregulation of the pressure-induced transcription factors. Overall, there are many possible explanations for the role that AP-2β plays in the development of SC, and further studies need to be conducted to gain a better understanding of its function.

Furthermore, it is interesting that SC simultaneously expresses both blood (Tie2) and lymphatic (Prox1) endothelial markers. This may provide further support for the theory that the structure continues to retain characteristics of both blood and lymphatic identities, rather than exhibiting attributes of each separately. Due to the fragility of ocular cryosections, it is difficult to make conclusions regarding the regions within SC that express Prox1 and Tie2. It is possible that Prox1 is more selectively expressed by the inner wall, and Tie2 by the outer wall, but further studies are required to investigate this further.

5.2. Effect of AP-2β deletion on the functionality of the uveoscleral pathway

Previously, we have reported an elevated baseline IOP in the AP-2β TMR-KO mutants, which reduced temporarily through treatment with latanaprost, a prostaglandin analog drug (Figure 9) (Taiyab et al., 2022). Latanaprost is known to decrease IOP by relaxing ciliary smooth muscle and remodeling the extracellular matrix of the uveoscleral pathway through increased metalloproteinases (Tripathy & Geetha, 2022). Since the conventional pathway is blocked in our AP-2β TMR-KO mutants due to absence of the trabecular meshwork and SC, we suspected that the decrease in IOP is due to the preserved functionality of the uveoscleral pathway. In order to confirm this, aqueous outflow was visualized through intracameral injections of a dextran tracer. In the wildtype, dextran was observed in regions associated with both the conventional and uveoscleral outflow

pathways in the untreated as well as 5 minutes post-latanaprost treatment eye; by the 10 minute treatment mark, most of the dextran was cleared out (Figure 21A-C). In the untreated mutant, dextran was clustered in the anterior chamber which was observed to flow out through the uveoscleral pathway 5 minutes after latanaprost treatment (Figure 21D-E). 10 minutes after latanaprost treatment, dextran was observed further along the uveoscleral pathway in the mutant (Figure 21F). Quantification of the fluorescent signal further confirmed these results as the signal in the anterior chamber of the untreated mutant was significantly greater than all other groups, which is consistent with the clustered dextran observed (Figure 22). The untreated control exhibited a significantly greater fluorescence signal in the region of the outflow pathways when compared to the untreated mutant, confirming that outflow in the mutant is blocked (Figure 23). Upon treatment, the signal in the anterior chamber of the mutant decreased and was reported at similar levels as the controls. These findings are in line with a previous study by Lindsey & Weinreb, where dextran injected in wildtype eyes was observed in the trabecular meshwork, ciliary processes, ciliary muscle, and choroid of mice, thus showing the existence of uveoscleral outflow in mice (Lindsey & Weinreb, 2002).

The results from this experiment demonstrate similarities between the AP-2β TMR-KO mutants and the presentation of closed-angle glaucoma in humans. This primarily includes closure of the iridocorneal angle, thus obstructing the drainage of aqueous humor and elevating IOP, also known as ocular hypertension. Drugs like latanaprost are then employed to reduce IOP by taking advantage of the uveoscleral pathway. Therefore, AP-

2β TMR-KO mouse model has the potential of being used as a model for glaucoma through which future studies can be conducted.

5.3. Future Directions and Conclusion

AP-2β deletion in the POM leads to defects in the structures involved in outflow of aqueous humor, as observed in the AP-2β TMR-KO mouse model recently developed in our laboratory. The trabecular meshwork and SC fail to develop in these mutants, thus blocking the conventional outflow pathway and leading to elevated IOP. The results of the experiments conducted in this project allow for a better understanding of the role of AP-2β in the development of SC. Future studies should be aimed at investigating whether the absence of pressure-induced markers like Prox1 and Klf4 is due to lack of flow through the SC region, or if AP-2β plays a more direct signaling role in regulating their expression. Attempts could be directed at creating a model in which pressure and flow can be manipulated, and expression of these markers can then be investigated. Additionally, the theory of crosstalk between the trabecular meshwork and SC through Angpt1-Tie2 signaling being crucial for SC development needs to be further explored. It is plausible that the failure of the trabecular meshwork to develop due to AP-2β deletion led to the absence of Angpt1 in the AP-2β TMR-KO mutants. However, this does not explain the absence of Tie2 observed in the SC region. The role of AP-2β in the expression of Tie2 and Angpt1 remains to be elucidated.

Additionally, the preserved uveoscleral outflow in conjunction with a blocked conventional pathway and elevated IOP exhibited by the AP-2β TMR-KO mutants point to the advantages of using these mice as a model for glaucoma. This model has the potential

to be employed for studies investigating the physiology and mechanism of IOP lowering drugs, as well as to explore novel neuroprotective drugs and strategies.

Overall, this project demonstrates that deletion of AP-2β from the developing POM leads to the absence of SC, thus disrupting aqueous outflow. This points to the importance of the role AP-2β expression plays in development, particularly ocular development. The phenotypes exhibited by the AP-2β TMR-KO mutants indicate the usefulness of the model as a model for glaucoma.

REFERENCES

Akula, M., Taiyab, A., Deschamps, P., Yee, S., Ball, A. K., Williams, T., & West-Mays, J. A. (2020). AP-2beta is required for formation of the murine trabecular meshwork and Schlemm's canal. *Exp Eye Res*, *195*, 108042. https://doi.org/10.1016/j.exer.2020.108042

Alm, A., & Stjernschantz, J. (1995). Effects on intraocular pressure and side effects of 0.005% latanoprost applied once daily, evening or morning. A comparison with timolol. Scandinavian Latanoprost Study Group. *Ophthalmology*, *102*(12), 1743-1752. https://doi.org/10.1016/s0161-6420(95)30798-1

Aspelund, A., Tammela, T., Antila, S., Nurmi, H., Leppanen, V. M., Zarkada, G., Stanczuk, L., Francois, M., Makinen, T., Saharinen, P., Immonen, I., & Alitalo, K. (2014). The Schlemm's canal is a VEGF-C/VEGFR-3-responsive lymphatic-like vessel. *J Clin Invest*, *124*(9), 3975-3986. https://doi.org/10.1172/JCI75395

Bassett, E. A., Korol, A., Deschamps, P. A., Buettner, R., Wallace, V. A., Williams, T., & West-Mays, J. A. (2012). Overlapping expression patterns and redundant roles for AP-2 transcription factors in the developing mammalian retina. *Dev Dyn*, *241*(4), 814-829. https://doi.org/10.1002/dvdy.23762

Bassett, E. A., Pontoriero, G. F., Feng, W., Marquardt, T., Fini, M. E., Williams, T., & West-Mays, J. A. (2007). Conditional deletion of activating protein 2alpha (AP-2alpha) in the developing retina demonstrates non-cell-autonomous roles for AP-2alpha in optic cup development. *Mol Cell Biol*, *27*(21), 7497-7510. https://doi.org/10.1128/MCB.00687-07

Bassett, E. A., Williams, T., Zacharias, A. L., Gage, P. J., Fuhrmann, S., & West-Mays, J. A. (2010). AP-2α knockout mice exhibit optic cup patterning defects and failure of optic stalk morphogenesis. *Human Molecular Genetics*, *19*(9), 1791-1804. https://doi.org/10.1093/hmg/ddq060

Bauer, R., Imhof, A., Pscherer, A., Kopp, H., Moser, M., Seegers, S., Kerscher, M., Tainsky, M. A., Hofstaedter, F., & Buettner, R. (1994). The genomic structure of the human AP-2 transcription factor. *Nucleic Acids Res*, *22*(8), 1413-1420. https://doi.org/10.1093/nar/22.8.1413

Berry, F. B., Lines, M. A., Oas, J. M., Footz, T., Underhill, D. A., Gage, P. J., & Walter, M. A. (2006). Functional interactions between FOXC1 and PITX2 underlie the sensitivity to FOXC1 gene dose in Axenfeld-Rieger syndrome and anterior segment dysgenesis. *Hum Mol Genet*, *15*(6), 905-919. https://doi.org/10.1093/hmg/ddl008

Bollinger, K. E., Crabb, J. S., Yuan, X., Putliwala, T., Clark, A. F., & Crabb, J. W. (2012). Proteomic similarities in steroid responsiveness in normal and glaucomatous trabecular meshwork cells. *Mol Vis*, *18*, 2001-2011. https://www.ncbi.nlm.nih.gov/pubmed/22876128

Borras, T., Smith, M. H., & Buie, L. K. (2015). A Novel Mgp-Cre Knock-In Mouse Reveals an Anticalcification/Antistiffness Candidate Gene in the Trabecular Meshwork and Peripapillary Scleral Region. *Invest Ophthalmol Vis Sci*, *56*(4), 2203-2214. https://doi.org/10.1167/iovs.15-16460

Braunger, B. M., Fuchshofer, R., & Tamm, E. R. (2015). The aqueous humor outflow pathways in glaucoma: A unifying concept of disease mechanisms and causative

treatment. *Eur J Pharm Biopharm*, *95*(Pt B), 173-181.
https://doi.org/10.1016/j.ejpb.2015.04.029

Chang, E. E., & Goldberg, J. L. (2012). Glaucoma 2.0: neuroprotection,
neuroregeneration, neuroenhancement. *Ophthalmology*, *119*(5), 979-986.
https://doi.org/10.1016/j.ophtha.2011.11.003

Chow, R. L., & Lang, R. A. (2001). Early eye development in vertebrates. *Annu Rev Cell Dev Biol*, *17*, 255-296. https://doi.org/10.1146/annurev.cellbio.17.1.255

Cvekl, A., & Tamm, E. R. (2004). Anterior eye development and ocular mesenchyme:
new insights from mouse models and human diseases. *Bioessays*, *26*(4), 374-386.
https://doi.org/10.1002/bies.20009

Dautriche, C. N., Tian, Y., Xie, Y., & Sharfstein, S. T. (2015). A Closer Look at
Schlemm's Canal Cell Physiology: Implications for Biomimetics. *J Funct
Biomater*, *6*(3), 963-985. https://doi.org/10.3390/jfb6030963

Duan, C., & Clemmons, D. R. (1995). Transcription factor AP-2 regulates human insulin-
like growth factor binding protein-5 gene expression. *J Biol Chem*, *270*(42),
24844-24851. https://doi.org/10.1074/jbc.270.42.24844

Eckert, D., Buhl, S., Weber, S., Jager, R., & Schorle, H. (2005). The AP-2 family of
transcription factors. *Genome Biol*, *6*(13), 246. https://doi.org/10.1186/gb-2005-6-
13-246

Ethier, C. R., Read, A. T., & Chan, D. (2004). Biomechanics of Schlemm's canal
endothelial cells: influence on F-actin architecture. *Biophys J*, *87*(4), 2828-2837.
https://doi.org/10.1529/biophysj.103.038133

Foets, B., van den Oord, J., Engelmann, K., & Missotten, L. (1992). A comparative
immunohistochemical study of human corneotrabecular tissue. *Graefes Arch Clin
Exp Ophthalmol*, *230*(3), 269-274. https://doi.org/10.1007/BF00176303

Gage, P. J., Rhoades, W., Prucka, S. K., & Hjalt, T. (2005). Fate Maps of Neural Crest
and Mesoderm in the Mammalian Eye. *Investigative Opthalmology & Visual
Science*, *46*(11), 4200. https://doi.org/10.1167/iovs.05-0691

Gage, P. J., Suh, H., & Camper, S. A. (1999). Dosage requirement of Pitx2 for
development of multiple organs. *Development*, *126*(20), 4643-4651.
https://doi.org/10.1242/dev.126.20.4643

Gaubatz, S., Imhof, A., Dosch, R., Werner, O., Mitchell, P., Buettner, R., & Eilers, M.
(1995). Transcriptional activation by Myc is under negative control by the
transcription factor AP-2. *EMBO J*, *14*(7), 1508-1519.
https://doi.org/10.1002/j.1460-2075.1995.tb07137.x

Gould, D. B., & John, S. W. (2002). Anterior segment dysgenesis and the developmental
glaucomas are complex traits. *Hum Mol Genet*, *11*(10), 1185-1193.
https://doi.org/10.1093/hmg/11.10.1185

Gould, D. B., Smith, R. S., & John, S. W. (2004). Anterior segment development relevant
to glaucoma. *Int J Dev Biol*, *48*(8-9), 1015-1029.
https://doi.org/10.1387/ijdb.041865dg

Grierson, I., Lee, W. R., Abraham, S., & Howes, R. C. (1978). Associations between the
cells of the walls of Schlemm's canal. *Albrecht Von Graefes Arch Klin Exp
Ophthalmol*, *208*(1-3), 33-47. https://doi.org/10.1007/BF00406980

Hagerling, R., Pollmann, C., Andreas, M., Schmidt, C., Nurmi, H., Adams, R. H., Alitalo, K., Andresen, V., Schulte-Merker, S., & Kiefer, F. (2013). A novel multistep mechanism for initial lymphangiogenesis in mouse embryos based on ultramicroscopy. *EMBO J*, *32*(5), 629-644. https://doi.org/10.1038/emboj.2012.340

Hamanaka, T., Bill, A., Ichinohasama, R., & Ishida, T. (1992). Aspects of the development of Schlemm's canal. *Exp Eye Res*, *55*(3), 479-488. https://doi.org/10.1016/0014-4835(92)90121-8

Hamanaka, T., Thornell, L. E., & Bill, A. (1997). Cytoskeleton and tissue origin in the anterior cynomolgus monkey eye. *Jpn J Ophthalmol*, *41*(3), 138-149. https://doi.org/10.1016/s0021-5155(97)00031-2

Heffner, C. S., Herbert Pratt, C., Babiuk, R. P., Sharma, Y., Rockwood, S. F., Donahue, L. R., Eppig, J. T., & Murray, S. A. (2012). Supporting conditional mouse mutagenesis with a comprehensive cre characterization resource. *Nat Commun*, *3*, 1218. https://doi.org/10.1038/ncomms2186

Hilger-Eversheim, K., Moser, M., Schorle, H., & Buettner, R. (2000). Regulatory roles of AP-2 transcription factors in vertebrate development, apoptosis and cell-cycle control. *Gene*, *260*(1-2), 1-12. https://doi.org/10.1016/s0378-1119(00)00454-6

Kass, M. A., Heuer, D. K., Higginbotham, E. J., Johnson, C. A., Keltner, J. L., Miller, J. P., Parrish, R. K., 2nd, Wilson, M. R., & Gordon, M. O. (2002). The Ocular Hypertension Treatment Study: a randomized trial determines that topical ocular hypotensive medication delays or prevents the onset of primary open-angle glaucoma. *Arch Ophthalmol*, *120*(6), 701-713; discussion 829-730. https://doi.org/10.1001/archopht.120.6.701

Kaufman, D. P., Sanvictores, T., & Costanza, M. (2022). Weibel Palade Bodies. In *StatPearls*. https://www.ncbi.nlm.nih.gov/pubmed/30570974

Kidson, S. H., Kume, T., Deng, K., Winfrey, V., & Hogan, B. L. (1999). The forkhead/winged-helix gene, Mf1, is necessary for the normal development of the cornea and formation of the anterior chamber in the mouse eye. *Dev Biol*, *211*(2), 306-322. https://doi.org/10.1006/dbio.1999.9314

Kim, J., Park, D. Y., Bae, H., Park, D. Y., Kim, D., Lee, C. K., Song, S., Chung, T. Y., Lim, D. H., Kubota, Y., Hong, Y. K., He, Y., Augustin, H. G., Oliver, G., & Koh, G. Y. (2017). Impaired angiopoietin/Tie2 signaling compromises Schlemm's canal integrity and induces glaucoma. *J Clin Invest*, *127*(10), 3877-3896. https://doi.org/10.1172/JCI94668

Kizhatil, K., Ryan, M., Marchant, J. K., Henrich, S., & John, S. W. (2014). Schlemm's canal is a unique vessel with a combination of blood vascular and lymphatic phenotypes that forms by a novel developmental process. *PLoS Biol*, *12*(7), e1001912. https://doi.org/10.1371/journal.pbio.1001912

Lewis, A. E., Vasudevan, H. N., O'Neill, A. K., Soriano, P., & Bush, J. O. (2013). The widely used Wnt1-Cre transgene causes developmental phenotypes by ectopic activation of Wnt signaling. *Dev Biol*, *379*(2), 229-234. https://doi.org/10.1016/j.ydbio.2013.04.026

Lin, C. R., Kioussi, C., O'Connell, S., Briata, P., Szeto, D., Liu, F., Izpisua-Belmonte, J. C., & Rosenfeld, M. G. (1999). Pitx2 regulates lung asymmetry, cardiac positioning and pituitary and tooth morphogenesis. *Nature*, *401*(6750), 279-282. https://doi.org/10.1038/45803

Lindsey, J. D., & Weinreb, R. N. (2002). Identification of the mouse uveoscleral outflow pathway using fluorescent dextran. *Invest Ophthalmol Vis Sci*, *43*(7), 2201-2205. https://www.ncbi.nlm.nih.gov/pubmed/12091417

Llobet, A., Gasull, X., & Gual, A. (2003). Understanding trabecular meshwork physiology: a key to the control of intraocular pressure? *News Physiol Sci*, *18*, 205-209. https://doi.org/10.1152/nips.01443.2003

Lutjen-Drecoll, E., & Rohen, J. W. (1970). [Endothelial studies of the Schlemm's canal using silver-impregnation technic]. *Albrecht Von Graefes Arch Klin Exp Ophthalmol*, *180*(4), 249-266. https://doi.org/10.1007/BF00414733 (Uber die endotheliale Auskleidung des Schlemmschen Kanals im Silberimpragnationsbild.)

Machiele, R., Motlagh, M., & Patel, B. C. (2020). Intraocular Pressure. In *StatPearls*. https://www.ncbi.nlm.nih.gov/pubmed/30335270

Martino, V. B., Sabljic, T., Deschamps, P., Green, R. M., Akula, M., Peacock, E., Ball, A., Williams, T., & West-Mays, J. A. (2016). Conditional deletion of AP-2beta in mouse cranial neural crest results in anterior segment dysgenesis and early-onset glaucoma. *Dis Model Mech*, *9*(8), 849-861. https://doi.org/10.1242/dmm.025262

McCormick, S. M., Eskin, S. G., McIntire, L. V., Teng, C. L., Lu, C. M., Russell, C. G., & Chittur, K. K. (2001). DNA microarray reveals changes in gene expression of shear stressed human umbilical vein endothelial cells. *Proc Natl Acad Sci U S A*, *98*(16), 8955-8960. https://doi.org/10.1073/pnas.171259298

McIntosh, I., Dreyer, S. D., Clough, M. V., Dunston, J. A., Eyaid, W., Roig, C. M., Montgomery, T., Ala-Mello, S., Kaitila, I., Winterpacht, A., Zabel, B., Frydman, M., Cole, W. G., Francomano, C. A., & Lee, B. (1998). Mutation analysis of LMX1B gene in nail-patella syndrome patients. *Am J Hum Genet*, *63*(6), 1651-1658. https://doi.org/10.1086/302165

Mitchell, P. J., Timmons, P. M., Hebert, J. M., Rigby, P. W., & Tjian, R. (1991). Transcription factor AP-2 is expressed in neural crest cell lineages during mouse embryogenesis. *Genes Dev*, *5*(1), 105-119. https://doi.org/10.1101/gad.5.1.105

Mohibullah, N., Donner, A., Ippolito, J. A., & Williams, T. (1999). SELEX and missing phosphate contact analyses reveal flexibility within the AP-2[alpha] protein: DNA binding complex. *Nucleic Acids Res*, *27*(13), 2760-2769. https://doi.org/10.1093/nar/27.13.2760

Moser, M., Pscherer, A., Roth, C., Becker, J., Mucher, G., Zerres, K., Dixkens, C., Weis, J., Guay-Woodford, L., Buettner, R., & Fassler, R. (1997). Enhanced apoptotic cell death of renal epithelial cells in mice lacking transcription factor AP-2beta. *Genes Dev*, *11*(15), 1938-1948. https://doi.org/10.1101/gad.11.15.1938

Moser, M., Ruschoff, J., & Buettner, R. (1997). Comparative analysis of AP-2 alpha and AP-2 beta gene expression during murine embryogenesis. *Dev Dyn*, *208*(1), 115-124. https://doi.org/10.1002/(SICI)1097-0177(199701)208:1<115::AID-AJA11>3.0.CO;2-5

Newman, S. P., Bates, N. P., Vernimmen, D., Parker, M. G., & Hurst, H. C. (2000). Cofactor competition between the ligand-bound oestrogen receptor and an intron 1 enhancer leads to oestrogen repression of ERBB2 expression in breast cancer. *Oncogene*, *19*(4), 490-497. https://doi.org/10.1038/sj.onc.1203416

Park, D. Y., Lee, J., Park, I., Choi, D., Lee, S., Song, S., Hwang, Y., Hong, K. Y., Nakaoka, Y., Makinen, T., Kim, P., Alitalo, K., Hong, Y. K., & Koh, G. Y. (2014). Lymphatic regulator PROX1 determines Schlemm's canal integrity and identity. *J Clin Invest*, *124*(9), 3960-3974. https://doi.org/10.1172/JCI75392

Pressman, C. L., Chen, H., & Johnson, R. L. (2000). LMX1B, a LIM homeodomain class transcription factor, is necessary for normal development of multiple tissues in the anterior segment of the murine eye. *Genesis*, *26*(1), 15-25. https://www.ncbi.nlm.nih.gov/pubmed/10660670

Quigley, H. A., & Broman, A. T. (2006). The number of people with glaucoma worldwide in 2010 and 2020. *Br J Ophthalmol*, *90*(3), 262-267. https://doi.org/10.1136/bjo.2005.081224

Ramos, R. F., Hoying, J. B., Witte, M. H., & Daniel Stamer, W. (2007). Schlemm's canal endothelia, lymphatic, or blood vasculature? *J Glaucoma*, *16*(4), 391-405. https://doi.org/10.1097/IJG.0b013e3180654ac6

Reneker, L. W., Silversides, D. W., Xu, L., & Overbeek, P. A. (2000). Formation of corneal endothelium is essential for anterior segment development - a transgenic mouse model of anterior segment dysgenesis. *Development*, *127*(3), 533-542. https://www.ncbi.nlm.nih.gov/pubmed/10631174

Satoda, M., Zhao, F., Diaz, G. A., Burn, J., Goodship, J., Davidson, H. R., Pierpont, M. E., & Gelb, B. D. (2000). Mutations in TFAP2B cause Char syndrome, a familial form of patent ductus arteriosus. *Nat Genet*, *25*(1), 42-46. https://doi.org/10.1038/75578

Schorle, H., Meier, P., Buchert, M., Jaenisch, R., & Mitchell, P. J. (1996). Transcription factor AP-2 essential for cranial closure and craniofacial development. *Nature*, *381*(6579), 235-238. https://doi.org/10.1038/381235a0

Smith, R. S., Zabaleta, A., Kume, T., Savinova, O. V., Kidson, S. H., Martin, J. E., Nishimura, D. Y., Alward, W. L., Hogan, B. L., & John, S. W. (2000). Haploinsufficiency of the transcription factors FOXC1 and FOXC2 results in aberrant ocular development. *Hum Mol Genet*, *9*(7), 1021-1032. https://doi.org/10.1093/hmg/9.7.1021

Souma, T., Tompson, S. W., Thomson, B. R., Siggs, O. M., Kizhatil, K., Yamaguchi, S., Feng, L., Limviphuvadh, V., Whisenhunt, K. N., Maurer-Stroh, S., Yanovitch, T. L., Kalaydjieva, L., Azmanov, D. N., Finzi, S., Mauri, L., Javadiyan, S., Souzeau, E., Zhou, T., Hewitt, A. W., . . . Young, T. L. (2016). Angiopoietin receptor TEK mutations underlie primary congenital glaucoma with variable expressivity. *J Clin Invest*, *126*(7), 2575-2587. https://doi.org/10.1172/JCI85830

Swamynathan, S. K., Davis, J., & Piatigorsky, J. (2008). Identification of candidate Klf4 target genes reveals the molecular basis of the diverse regulatory roles of Klf4 in the mouse cornea. *Invest Ophthalmol Vis Sci*, *49*(8), 3360-3370. https://doi.org/10.1167/iovs.08-1811

Taiyab, A., Akula, M., Dham, J., Deschamps, P., Sheardown, H., Williams, T., Borras, T., & West-Mays, J. A. (2022). Deletion of transcription factor AP-2beta from the developing murine trabecular meshwork region leads to progressive glaucomatous changes. *J Neurosci Res*, *100*(2), 638-652. https://doi.org/10.1002/jnr.24982

Thomson, B. R., Liu, P., Onay, T., Du, J., Tompson, S. W., Misener, S., Purohit, R. R., Young, T. L., Jin, J., & Quaggin, S. E. (2021). Cellular crosstalk regulates the aqueous humor outflow pathway and provides new targets for glaucoma therapies. *Nat Commun*, *12*(1), 6072. https://doi.org/10.1038/s41467-021-26346-0

Thomson, B. R., Souma, T., Tompson, S. W., Onay, T., Kizhatil, K., Siggs, O. M., Feng, L., Whisenhunt, K. N., Yanovitch, T. L., Kalaydjieva, L., Azmanov, D. N., Finzi, S., Tanna, C. E., Hewitt, A. W., Mackey, D. A., Bradfield, Y. S., Souzeau, E., Javadiyan, S., Wiggs, J. L., . . . Quaggin, S. E. (2017). Angiopoietin-1 is required for Schlemm's canal development in mice and humans. *J Clin Invest*, *127*(12), 4421-4436. https://doi.org/10.1172/JCI95545

Tripathy, K., & Geetha, R. (2022). Latanoprost. In *StatPearls*. https://www.ncbi.nlm.nih.gov/pubmed/31082022

Truong, T. N., Li, H., Hong, Y. K., & Chen, L. (2014). Novel characterization and live imaging of Schlemm's canal expressing Prox-1. *PLoS One*, *9*(5), e98245. https://doi.org/10.1371/journal.pone.0098245

Wankhade, S., Yu, Y., Weinberg, J., Tainsky, M. A., & Kannan, P. (2000). Characterization of the activation domains of AP-2 family transcription factors. *J Biol Chem*, *275*(38), 29701-29708. https://doi.org/10.1074/jbc.M000931200

Weinreb, R. N., Aung, T., & Medeiros, F. A. (2014). The pathophysiology and treatment of glaucoma: a review. *JAMA*, *311*(18), 1901-1911. https://doi.org/10.1001/jama.2014.3192

Werling, U., & Schorle, H. (2002). Transcription factor gene AP-2 gamma essential for early murine development. *Mol Cell Biol*, *22*(9), 3149-3156. https://doi.org/10.1128/MCB.22.9.3149-3156.2002

West-Mays, J. A., Zhang, J., Nottoli, T., Hagopian-Donaldson, S., Libby, D., Strissel, K. J., & Williams, T. (1999). AP-2alpha transcription factor is required for early morphogenesis of the lens vesicle. *Dev Biol*, *206*(1), 46-62. https://doi.org/10.1006/dbio.1998.9132

Williams, A. L., & Bohnsack, B. L. (2015). Neural crest derivatives in ocular development: discerning the eye of the storm. *Birth Defects Res C Embryo Today*, *105*(2), 87-95. https://doi.org/10.1002/bdrc.21095

Zhang, J., Hagopian-Donaldson, S., Serbedzija, G., Elsemore, J., Plehn-Dujowich, D., McMahon, A. P., Flavell, R. A., & Williams, T. (1996). Neural tube, skeletal and body wall defects in mice lacking transcription factor AP-2. *Nature*, *381*(6579), 238-241. https://doi.org/10.1038/381238a0